Fragmentation Functions at Belle and Belle II

KATHERINE PARHAM

Duke
Nuclear
Structure

U.S. DEPARTMENT OF
ENERGY
Office of
Science

Graduate Research
Fellowship Program

Duke
UNIVERSITY

BELLE II EXPERIMENT

THE DETECTOR

- The upgraded Belle II began taking data in 2019:
  - **Vertex Detector (VXD)**: two innermost silicon strips replaced with pixel detectors
  - **Central Drift Chamber (CDC)**: smaller drift cells, reaches smaller radii
  - **Time Of Propagation (TOP)**: replaced TOF
  - **Aerogel Ring Imaging Cherenkov Detector (ARICH)**: replaced endcap ACC
  - **Electromagnetic Calorimeter (ECL)**: electronics upgrade
  - **K_L Muon Detector (KLM)**: two innermost barrel RPCs and endcaps replaced with scintillators

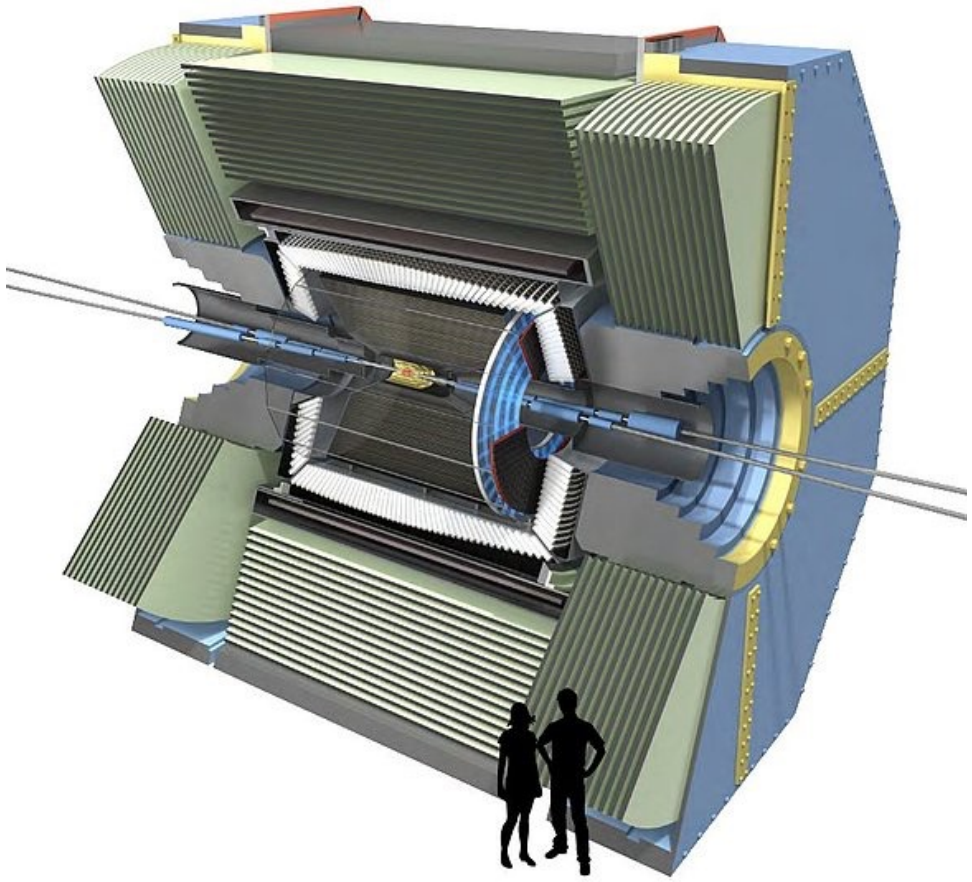

BELLE II EXPERIMENT

THE DETECTOR

- The upgraded Belle II began taking data in 2019:
  - **Vertex Detector (VXD)**: two innermost silicon strips replaced with pixel detectors
  - **Central Drift Chamber (CDC)**: smaller drift cells, reaches smaller radii
  - **Time Of Propagation (TOP)**: replaced TOF
  - **Aerogel Ring Imaging Cherenkov Detector (ARICH)**: replaced endcap ACC
  - **Electromagnetic Calorimeter (ECL)**: electronics upgrade
  - **K_L Muon Detector (KLM)**: two innermost barrel RPCs and endcaps replaced with scintillators

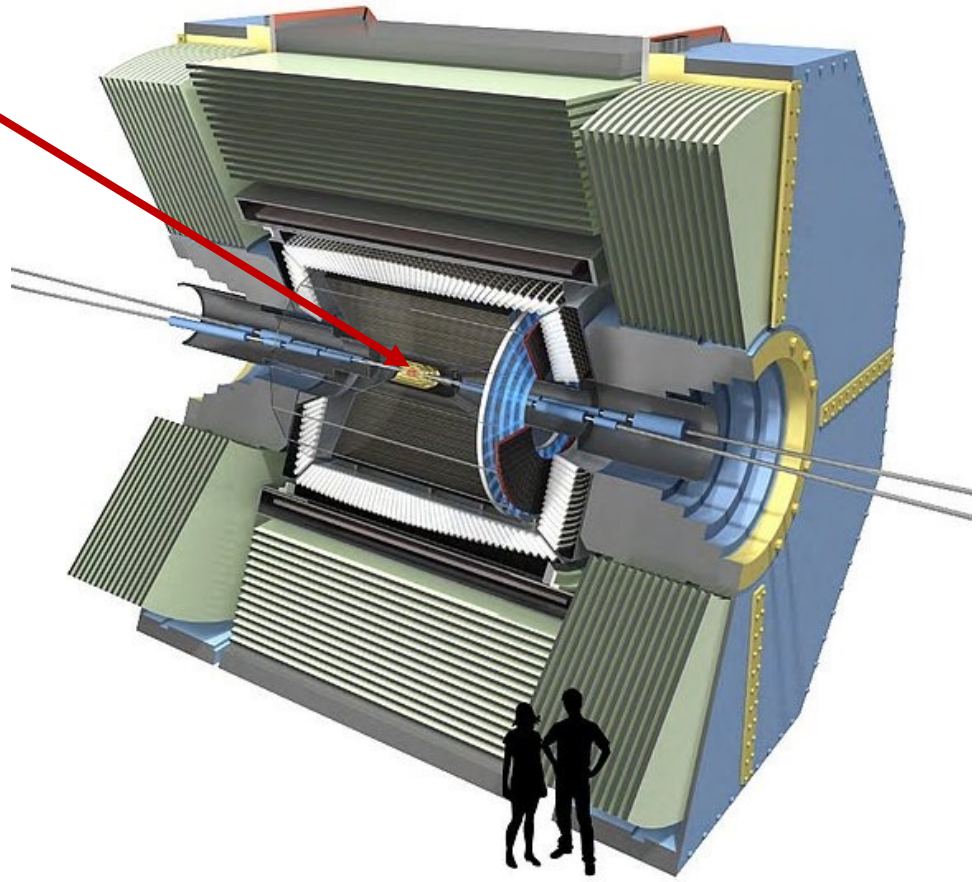

BELLE II EXPERIMENT

THE DETECTOR

- The upgraded Belle II began taking data in 2019:
  - **Vertex Detector (VXD)**: two innermost silicon strips replaced with pixel detectors
  - **Central Drift Chamber (CDC)**: smaller drift cells, reaches smaller radii
  - **Time Of Propagation (TOP)**: replaced TOF
  - **Aerogel Ring Imaging Cherenkov Detector (ARICH)**: replaced endcap ACC
  - **Electromagnetic Calorimeter (ECL)**: electronics upgrade
  - **K_L Muon Detector (KLM)**: two innermost barrel RPCs and endcaps replaced with scintillators

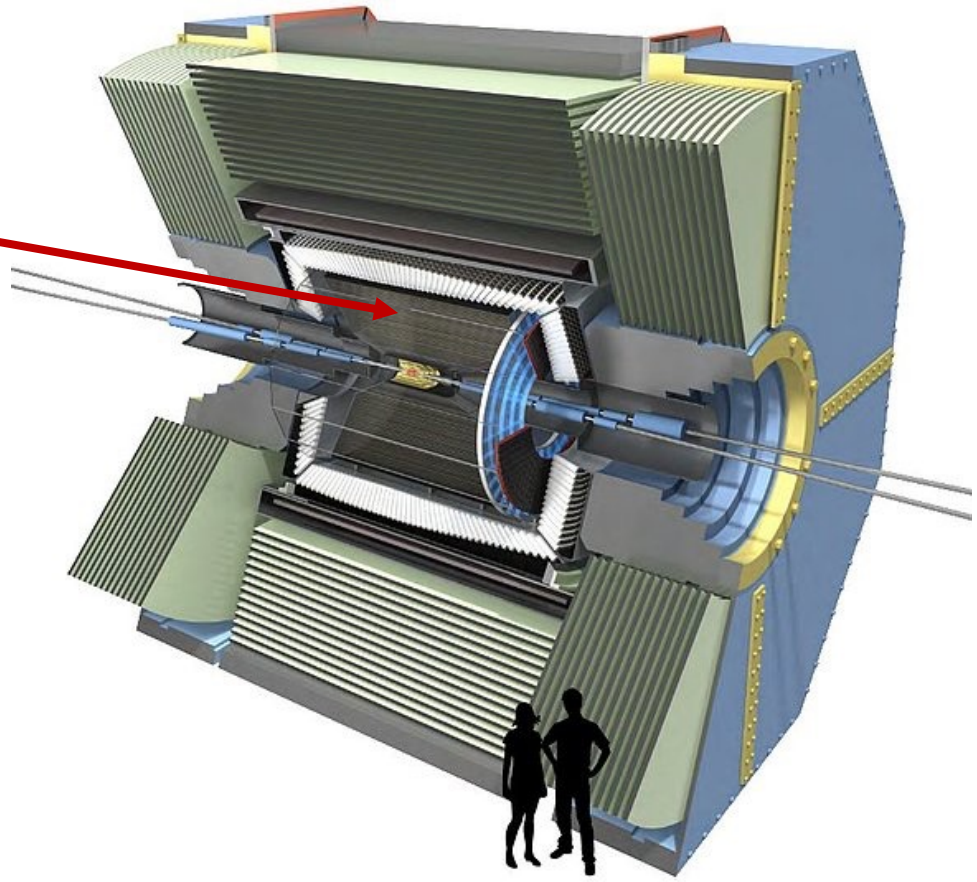

BELLE II EXPERIMENT

THE DETECTOR

- The upgraded Belle II began taking data in 2019:
  - **Vertex Detector (VXD)**: two innermost silicon strips replaced with pixel detectors
  - **Central Drift Chamber (CDC)**: smaller drift cells, reaches smaller radii
  - **Time Of Propagation (TOP)**: replaced TOF
  - **Aerogel Ring Imaging Cherenkov Detector (ARICH)**: replaced endcap ACC
  - **Electromagnetic Calorimeter (ECL)**: electronics upgrade
  - **K_L Muon Detector (KLM)**: two innermost barrel RPCs and endcaps replaced with scintillators

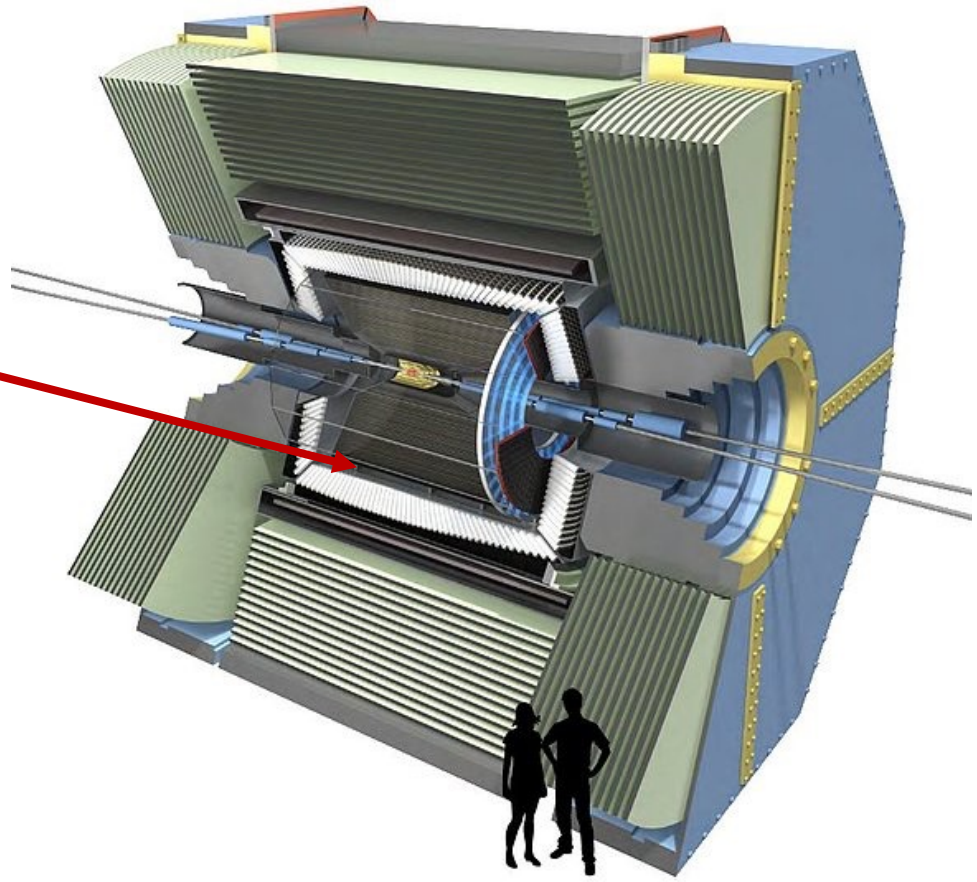

BELLE II EXPERIMENT

THE DETECTOR

- The upgraded Belle II began taking data in 2019:
  - **Vertex Detector (VXD)**: two innermost silicon strips replaced with pixel detectors
  - **Central Drift Chamber (CDC)**: smaller drift cells, reaches smaller radii
  - **Time Of Propagation (TOP)**: replaced TOF
  - **Aerogel Ring Imaging Cherenkov Detector (ARICH)**: replaced endcap ACC
  - **Electromagnetic Calorimeter (ECL)**: electronics upgrade
  - **K_L Muon Detector (KLM)**: two innermost barrel RPCs and endcaps replaced with scintillators

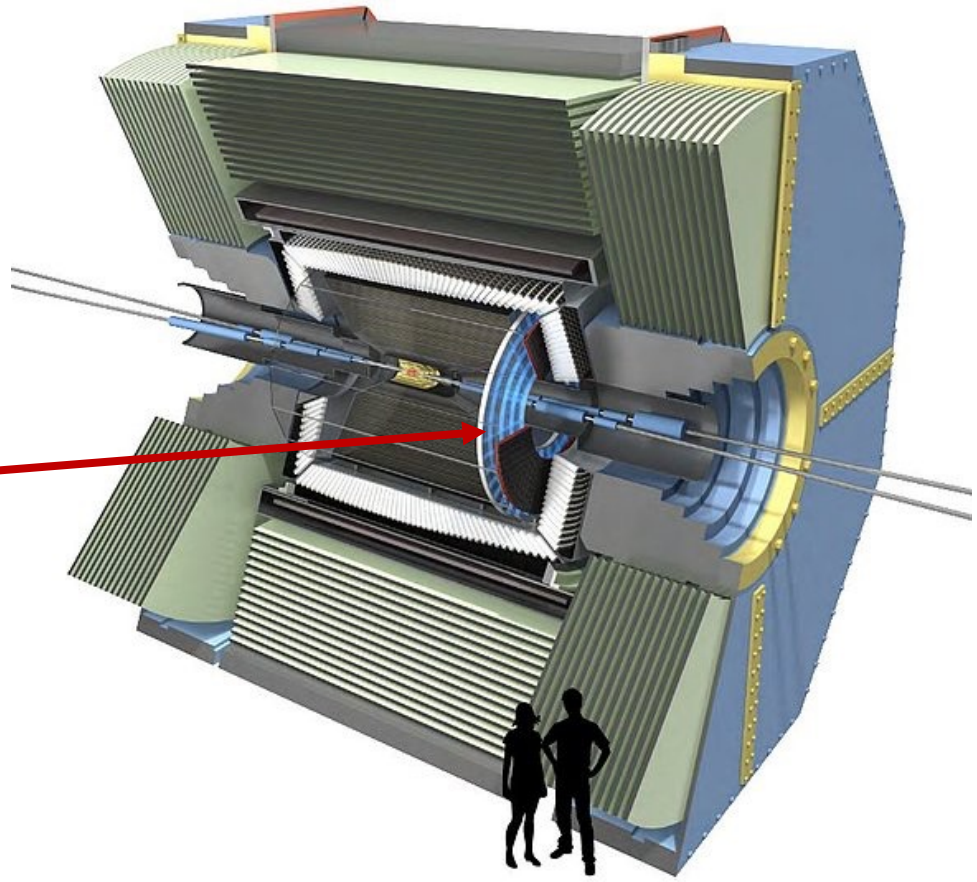

BELLE II EXPERIMENT

THE DETECTOR

- The upgraded Belle II began taking data in 2019:
  - **Vertex Detector (VXD)**: two innermost silicon strips replaced with pixel detectors
  - **Central Drift Chamber (CDC)**: smaller drift cells, reaches smaller radii
  - **Time Of Propagation (TOP)**: replaced TOF
  - **Aerogel Ring Imaging Cherenkov Detector (ARICH)**: replaced endcap ACC
  - **Electromagnetic Calorimeter (ECL)**: electronics upgrade
  - **K_L Muon Detector (KLM)**: two innermost barrel RPCs and endcaps replaced with scintillators

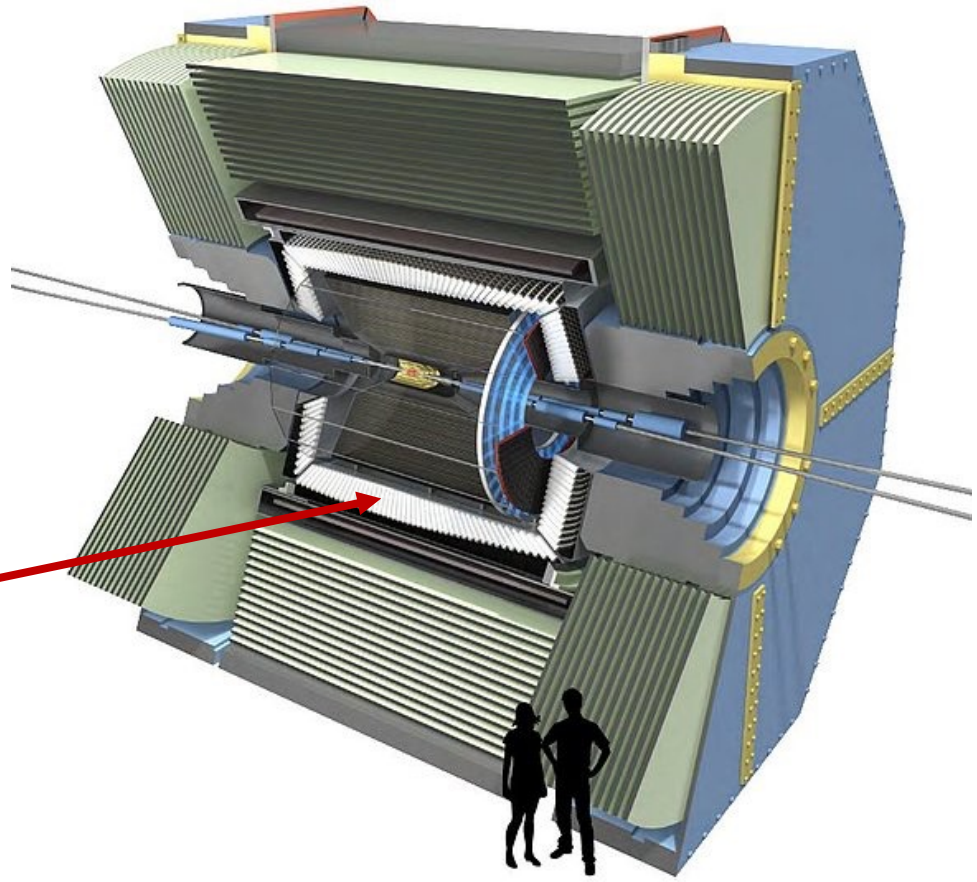

BELLE II EXPERIMENT

THE DETECTOR

- The upgraded Belle II began taking data in 2019:
  - **Vertex Detector (VXD)**: two innermost silicon strips replaced with pixel detectors
  - **Central Drift Chamber (CDC)**: smaller drift cells, reaches smaller radii
  - **Time Of Propagation (TOP)**: replaced TOF
  - **Aerogel Ring Imaging Cherenkov Detector (ARICH)**: replaced endcap ACC
  - **Electromagnetic Calorimeter (ECL)**: electronics upgrade
  - **K_L Muon Detector (KLM)**: two innermost barrel RPCs and endcaps replaced with scintillators

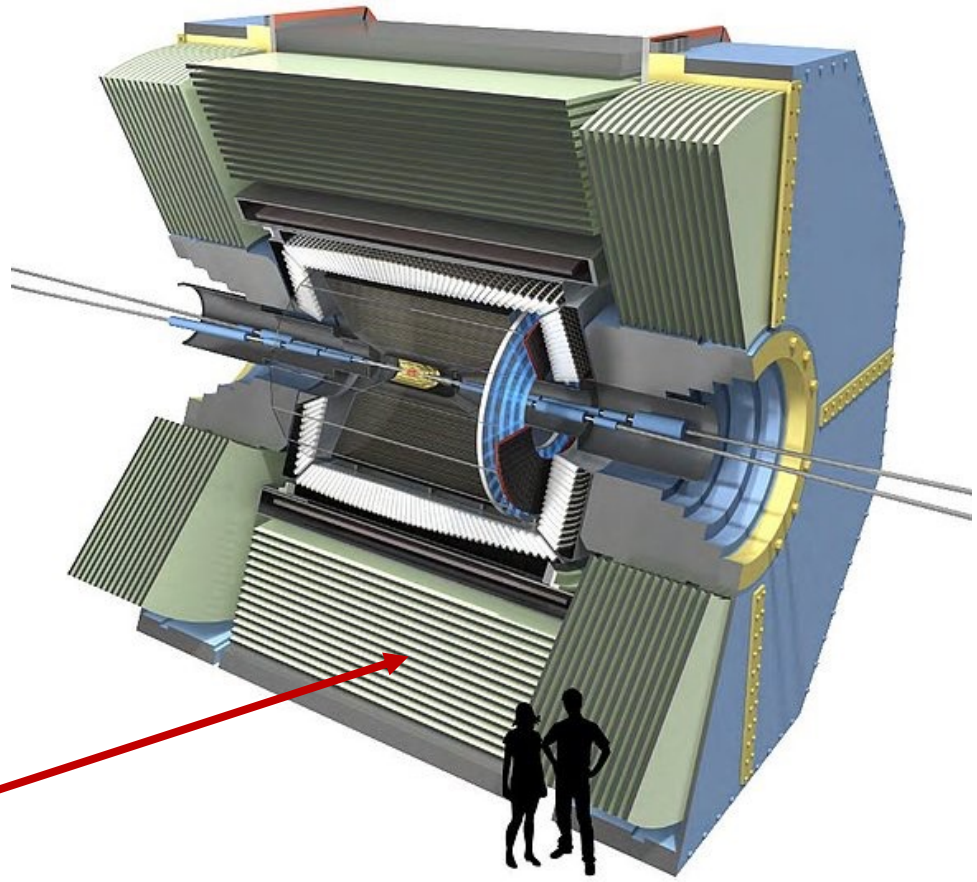

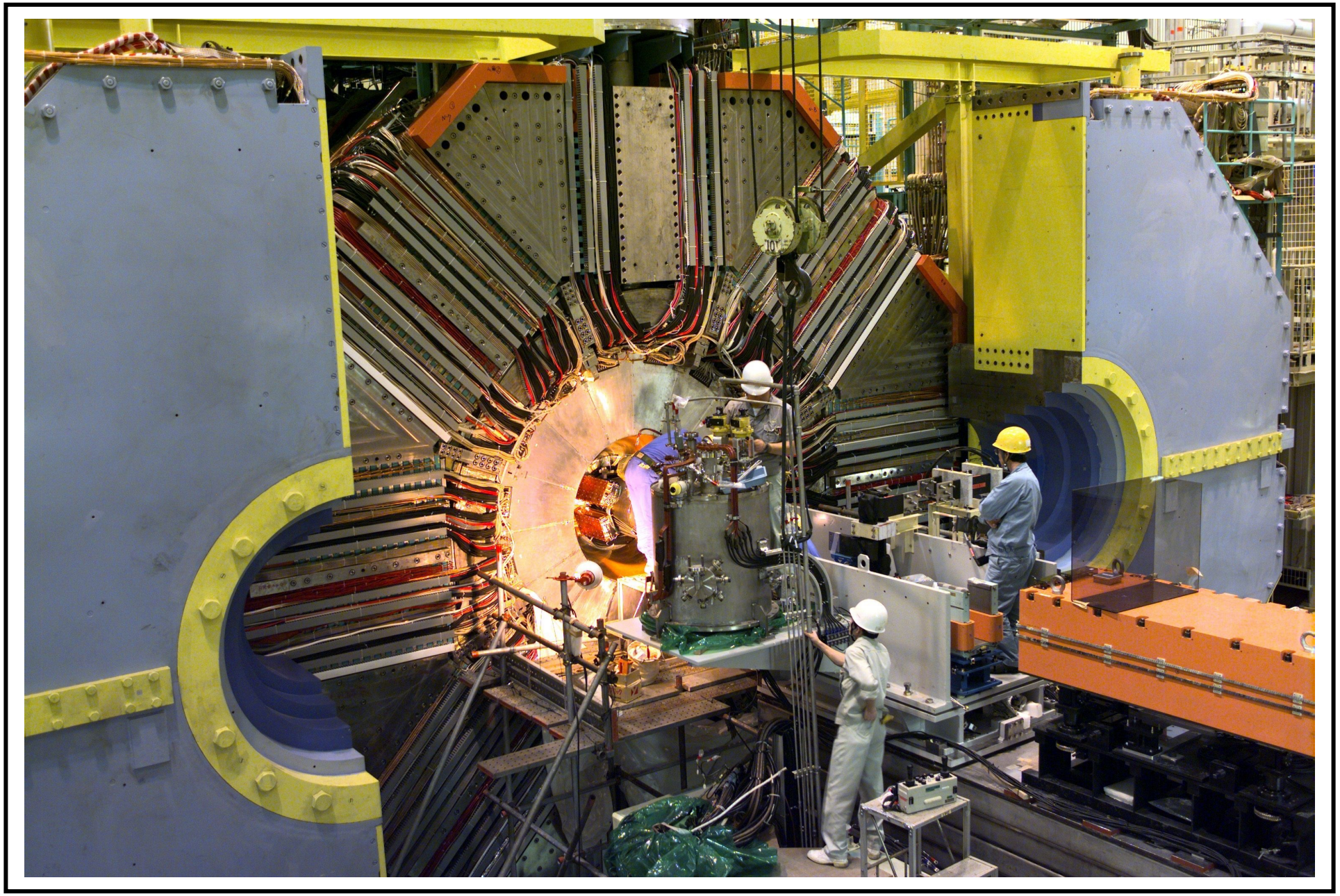

BELLE II

BELLE II EXPERIMENT

THE ACCELERATOR

- Located at the SuperKEKB accelerator in Tsukuba, Japan
- Designed to study e+ e- annihilation at the Υ(4S) resonance
- Upgrades from KEKB to SuperKEKB
  - Increased target beam current, roughly doubled from KEKB
  - Nanobeam collision scheme
- Set world record for instantaneous luminosity at $4.7 \times 10^{34}\ cm^{-2}s^{-1}$
- Total Integrated Luminosity
  - BaBar: $514\ fb^{-1}$
  - Belle: $1040\ fb^{-1}$
  - Belle II: $424\ fb^{-1}$

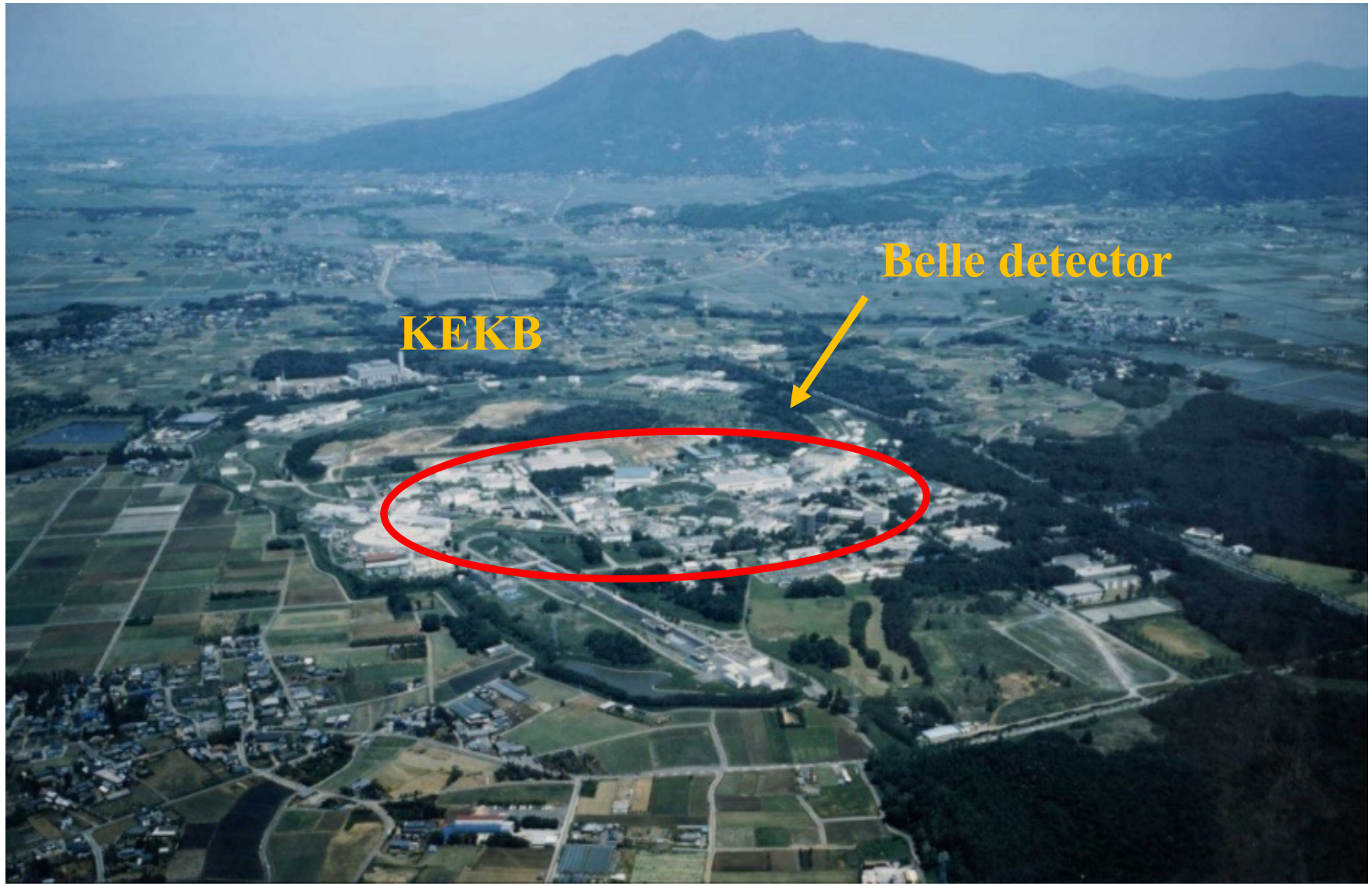

AERIAL VIEW OF EXPERIMENT

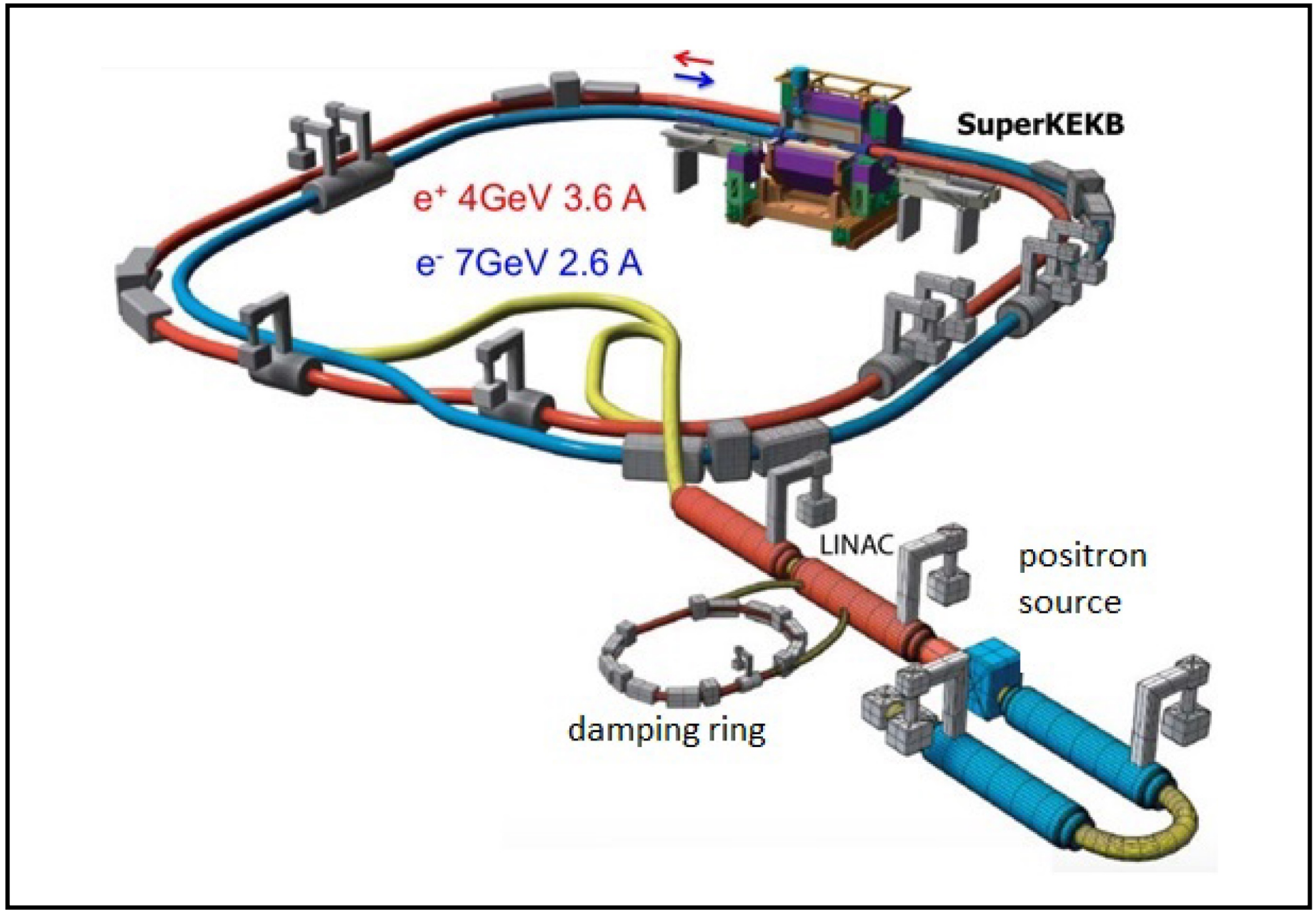
SuperKEKB
e+ 4GeV 3.6 A
e- 7GeV 2.6 A
LINAC
positron
source
damping ring

SUPERKEKB

BELLE II EXPERIMENT

THE ACCELERATOR

- Located at the SuperKEKB accelerator in Tsukuba, Japan
- Designed to study e+ e- annihilation at the Υ(4S) resonance
- Upgrades from KEKB to SuperKEKB
  - Increased target beam current, roughly doubled from KEKB
  - Nanobeam collision scheme
- Set world record for instantaneous luminosity at $4.2 \times 10^{34}\ cm^{-2}s^{-1}$
- Total Integrated Luminosity
  - BaBar: $513.7\ fb^{-1}$
  - Belle: $1040\ fb^{-1}$
  - Belle II: $427.8\ fb^{-1}$

FRAGMENTATION FUNCTIONS

DEFINITIONS

Hadronization: the process by which a parton produces a jet

FRAGMENTATION FUNCTIONS

DEFINITIONS

Hadronization: the process by which a parton produces a jet

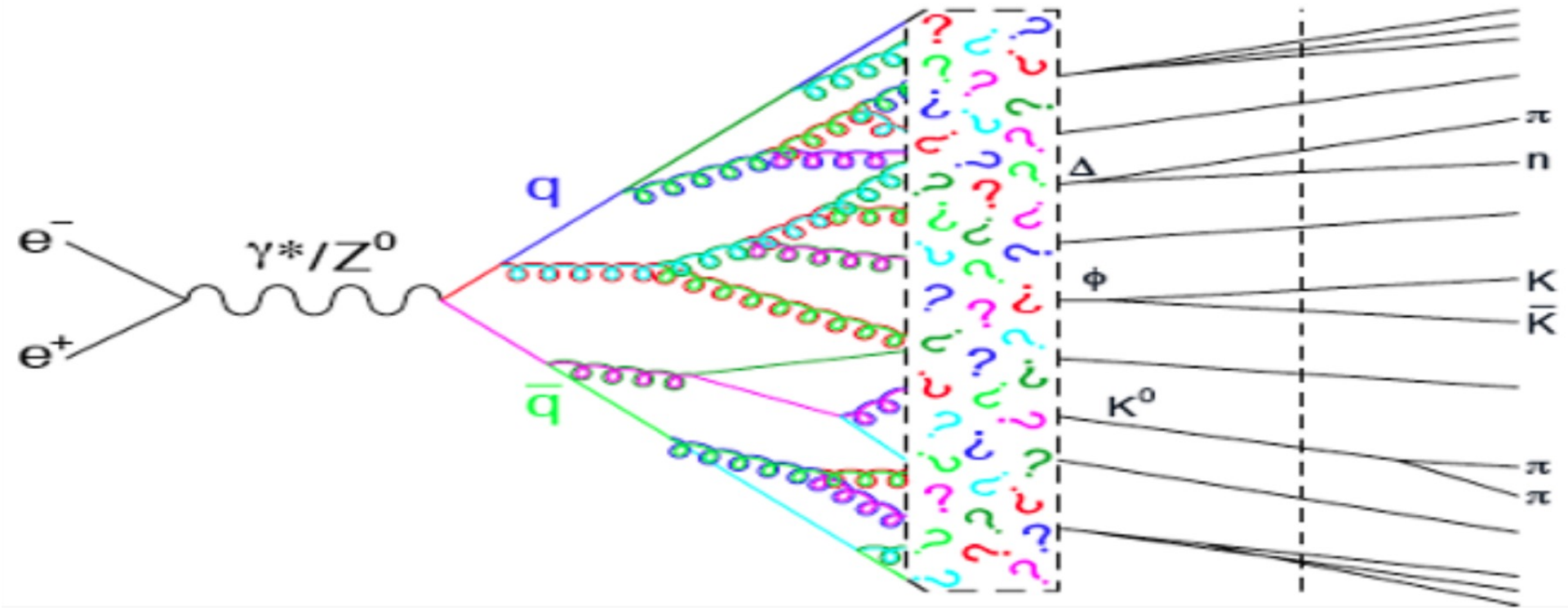

FRAGMENTATION FUNCTIONS

DEFINITIONS

Hadronization: the process by which a parton produces a jet

Fragmentation functions (FF): describe how color carrying quarks fragment into color neutral hadrons

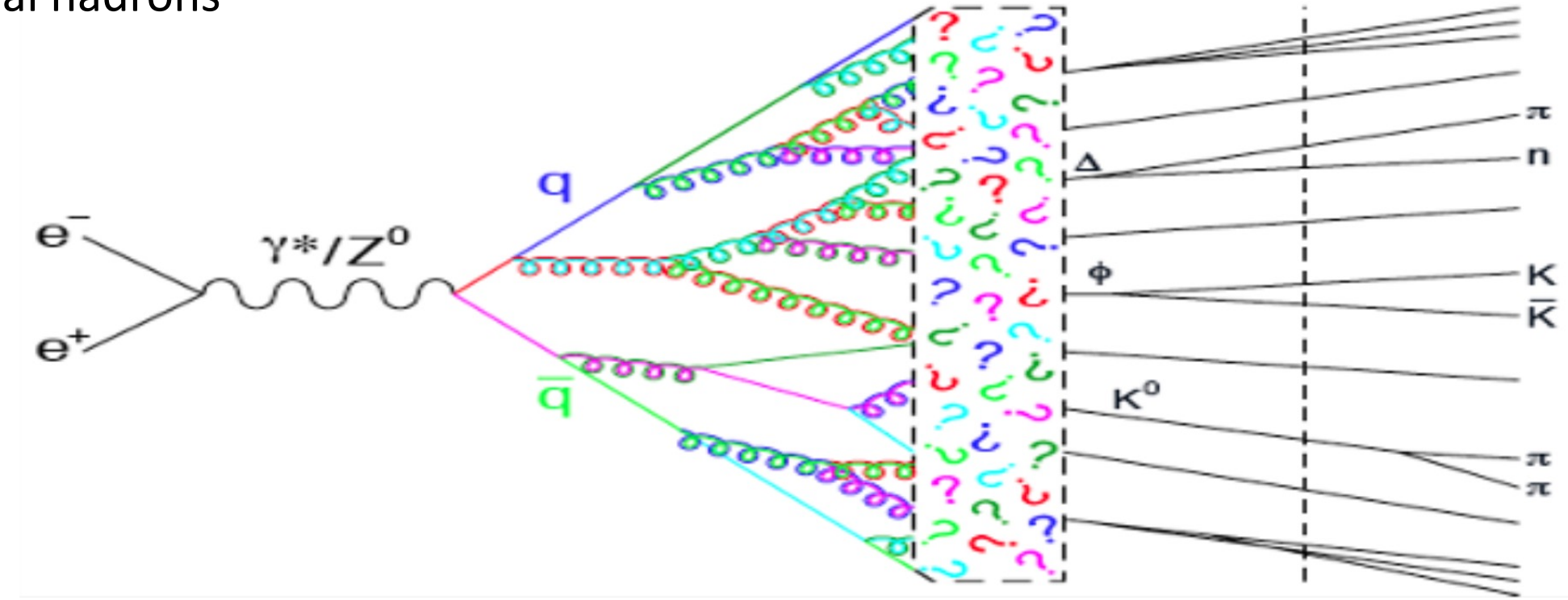

FRAGMENTATION FUNCTIONS

FACTORIZATION

Scattering amplitudes can be factorized into a perturbatively calculable part, $\hat{\sigma}$, and a non-perturbatively calculable part:

Single-inclusive annihilation:

$\sigma^{e^+e^-\to hX} = \hat{\sigma} \otimes FF$

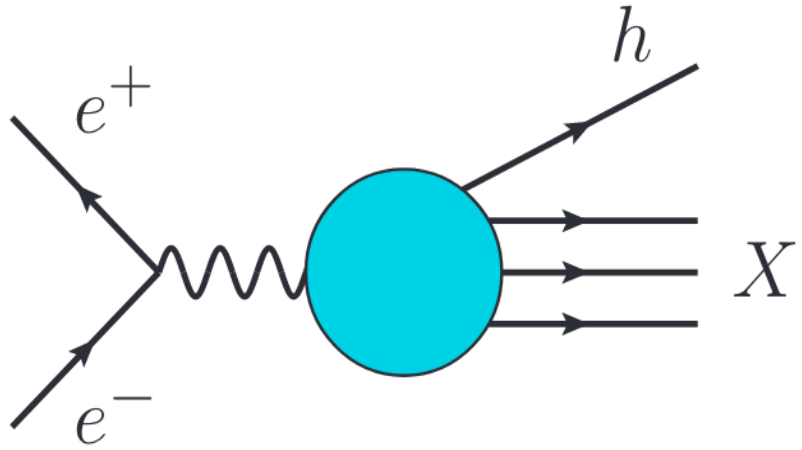

Semi-inclusive deep inelastic scattering (SIDIS):

$\sigma^{\ell N\to \ell hX} = \hat{\sigma} \otimes PDF \otimes FF$

Single-inclusive proton-proton scattering:

$\sigma^{pp\to hX} = \hat{\sigma} \otimes PDF \otimes PDF \otimes FF$

FRAGMENTATION FUNCTIONS

FACTORIZATION

Scattering amplitudes can be factorized into a perturbatively calculable part, $\hat{\sigma}$, and a non-perturbatively calculable part:

Single-inclusive annihilation:

$\sigma^{e^+e^-\to hX} = \hat{\sigma} \otimes FF$

Semi-inclusive deep inelastic scattering (SIDIS):

$\sigma^{\ell N\to \ell hX} = \hat{\sigma} \otimes PDF \otimes FF$

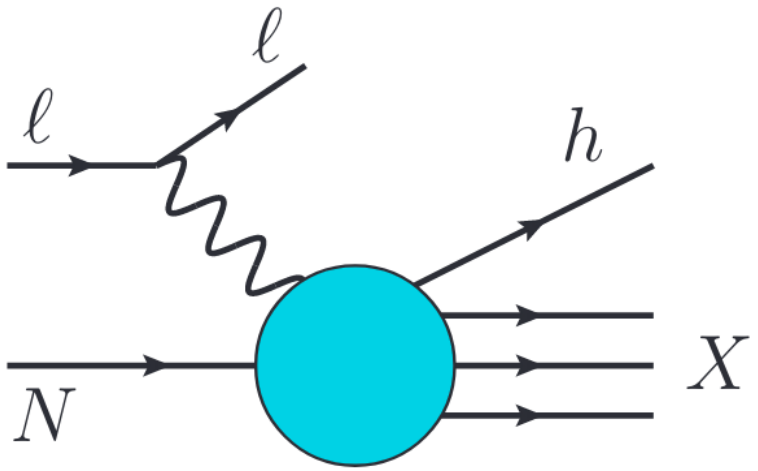

Single-inclusive proton-proton scattering:

$\sigma^{pp\to hX} = \hat{\sigma} \otimes PDF \otimes PDF \otimes FF$

FRAGMENTATION FUNCTIONS

FACTORIZATION

Scattering amplitudes can be factorized into a perturbatively calculable part, $\hat{\sigma}$, and a non-perturbatively calculable part:

Single-inclusive annihilation:

$$\sigma^{e^+e^-\to hX} = \hat{\sigma} \otimes FF$$

Semi-inclusive deep inelastic scattering (SIDIS):

$$\sigma^{\ell N\to \ell hX} = \hat{\sigma} \otimes PDF \otimes FF$$

Single-inclusive proton-proton scattering:

$$\sigma^{pp\to hX} = \hat{\sigma} \otimes PDF \otimes PDF \otimes FF$$

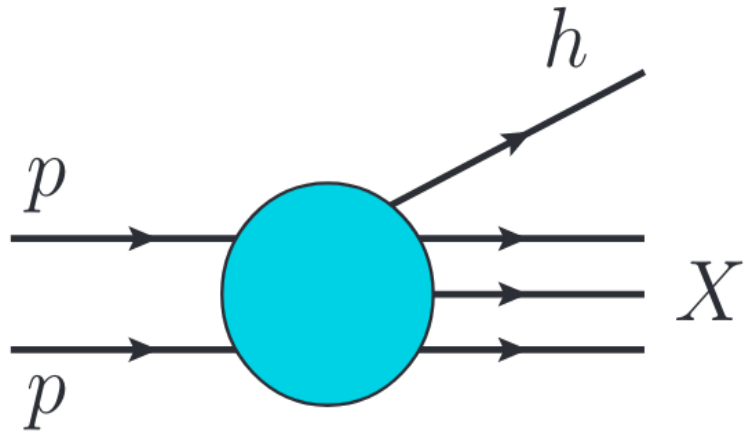

R. Seidl et al., "Update of inclusive cross sections of single and pairs of identified light charged hadrons", *Phys.Rev.D* 101 (2020) 9, 092004

- Used an updated ISR correction procedure
- Alternative fractional energy definitions were considered
  - Conventional: $z_i = 2E_{h,i} / \sqrt{s}$
  - AEMP: $z_1 = \frac{2P_1 \cdot q}{q^2}$, $z_2 = \frac{P_1 \cdot P_2}{P_1 \cdot q}$
  - MVH: $z_1 = \left(P_1 \cdot P_2 - \frac{M_{h1}^2 M_{h2}^2}{P_1 \cdot P_2}\right) \frac{1}{P_2 \cdot q - M_{h2}^2 \frac{P_1 \cdot q}{P_1 \cdot P_2}}$,

$$z_2 = \left(P_2 \cdot P_1 - \frac{M_{h2}^2 M_{h1}^2}{P_2 \cdot P_1}\right) \frac{1}{P_1 \cdot q - M_{h1}^2 \frac{P_2 \cdot q}{P_2 \cdot P_1}}$$

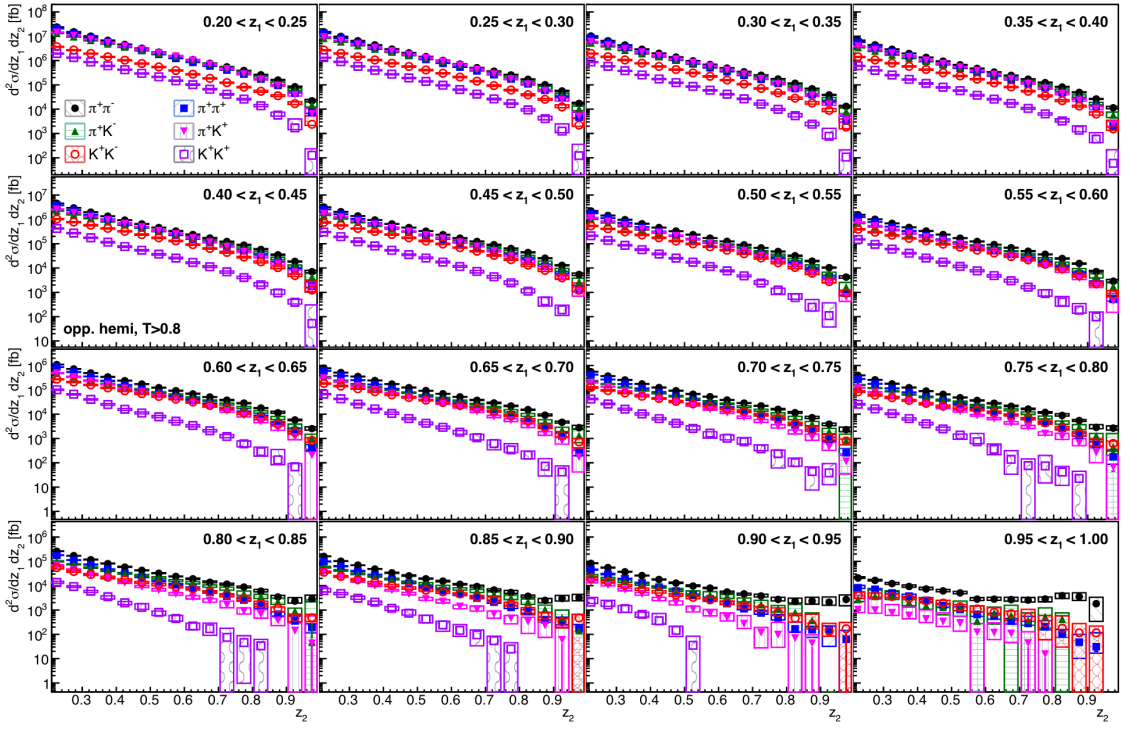

Differential cross sections of charged hadron pairs in opposite hemispheres, binned by conventional fractional energy

BELLE RESULTS

RECENT PUBLICATIONS

H. Li, A. Vossen, et al., "Azimuthal asymmetries of back-to-back $\pi^{\pm} - (\pi^0, \eta, \pi^{\pm})$ pairs in e^+e^- annihilation", *Phys.Rev.D* 100 (2019) 9, 092008

- The first observation of azimuthal asymmetries of pairs of back-to-back hadrons, one a charged pion and the other a π^0, $\pi^{\pm}$, or η meson
- Measurements are sensitive to the Collins fragmentation function, $H_1^{\perp}$

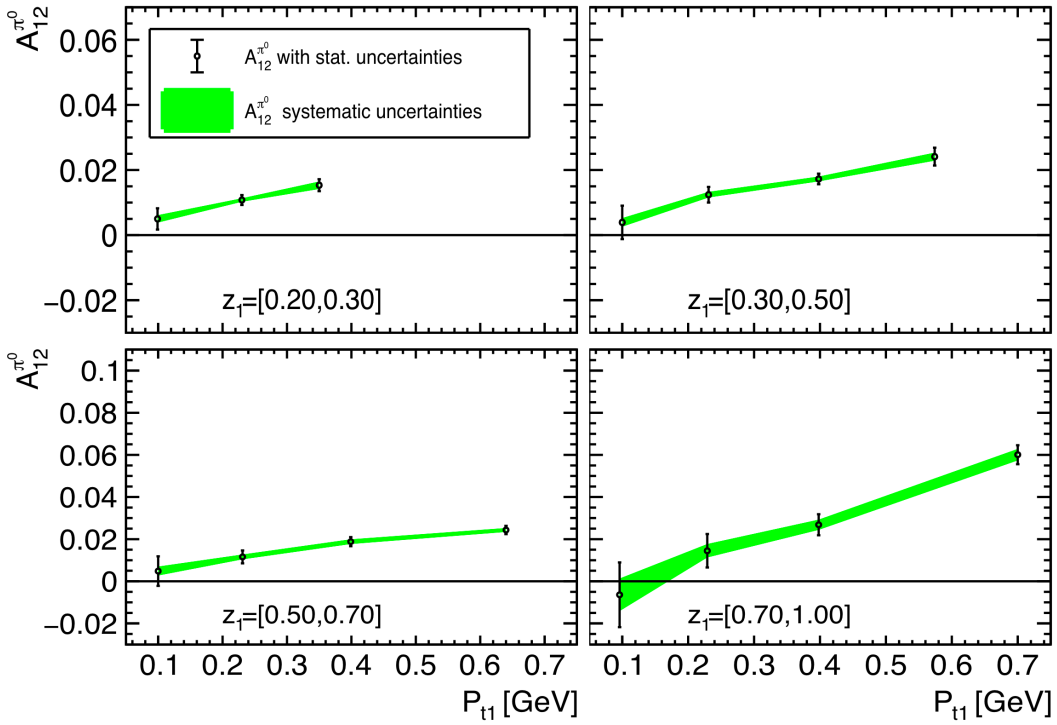

Azimuthal asymmetry of π^0 events binned by fractional energy, z

R. Seidl et al., "Transverse momentum dependent production cross sections of charged pions, kaons and protons produced in inclusive e^+e^- annihilation at $\sqrt{s}$ = 10.58 GeV", *Phys.Rev.D* 99 (2019) 11, 112006

- Production cross sections of charged pions, kaons, and protons as a function of fractional energy, thrust, and transverse momentum
- Measurements access the transverse momenta created during fragmentation

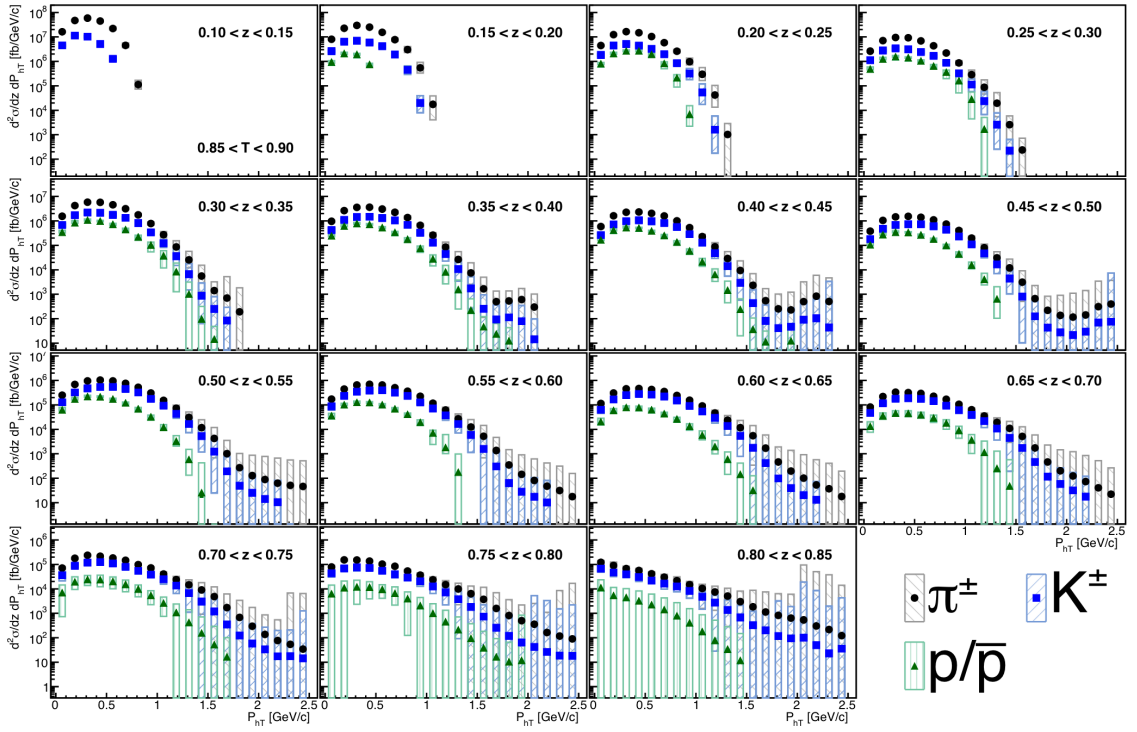

Differential cross sections as a function of transverse momentum

ONGOING RESEARCH

BELLE | $H_1^{\sphericalangle}$ DiFF | JET FUNCTIONS

Explicit cross-sections for vector mesons and D mesons

- R. Seidl
- Measurement of vector meson and heavy quark fragmentation
- These cross-sections can also be used to correct FF measurements that include weak decays

Back-to-back di-hadron TMD measurements

- A. Vossen, C. Van Hulse
- Sensitive to the single hadron TMD FF
- The second hadron provides an axis with which to measure P_{hT}

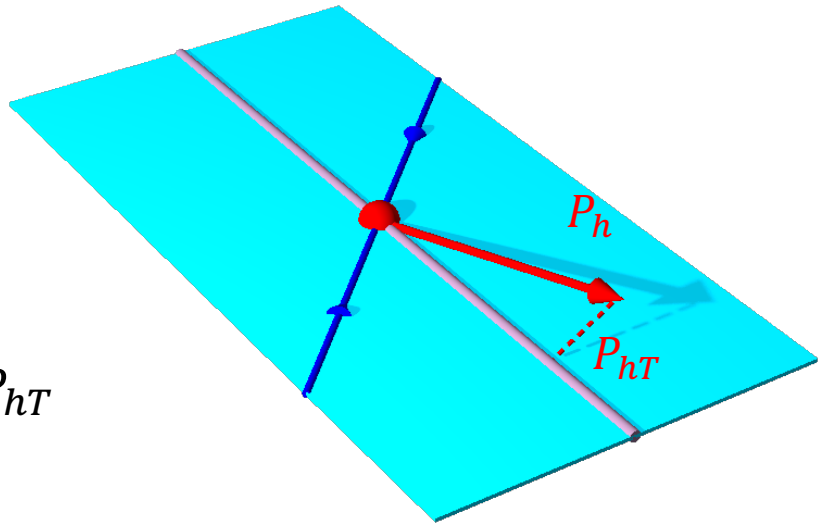

ONGOING RESEARCH

BELLE | $H_1^{\sphericalangle}$ DiFF | JET FUNCTIONS

- Di-hadron fragmentation functions (DiFF): describe the fragmentation of a quark into a pair of hadrons
- DiFFs were originally introduced to describe jet structure
  - Jet handedness: an observable that is proportional to the polarization of the parent parton
- $H_1^{\sphericalangle}$ describes the fragmentation of a polarized quark into a pair of spin-0 hadrons
  - Related to transverse jet handedness
  - Considered an interference fragmentation function (IFF)
  - Quark spin polarimeter: Determines the transverse spin states of final state quarks

ONGOING RESEARCH

BELLE | $H_1^{\sphericalangle}$ DiFF | JET FUNCTIONS

- The $H_1^{\sphericalangle}$ FF describes the production of a pair of spin-0 hadrons
- Conservation of angular momentum leads to left and right asymmetry
- The spin correlation between a quark-antiquark pair leads to a correlation between the azimuthal angle of the di-hadron pairs it produces
- The amplitude of the resulting asymmetry in the azimuthal angle is directly proportional to $H_1^{\sphericalangle}\overline{H_1^{\sphericalangle}}$

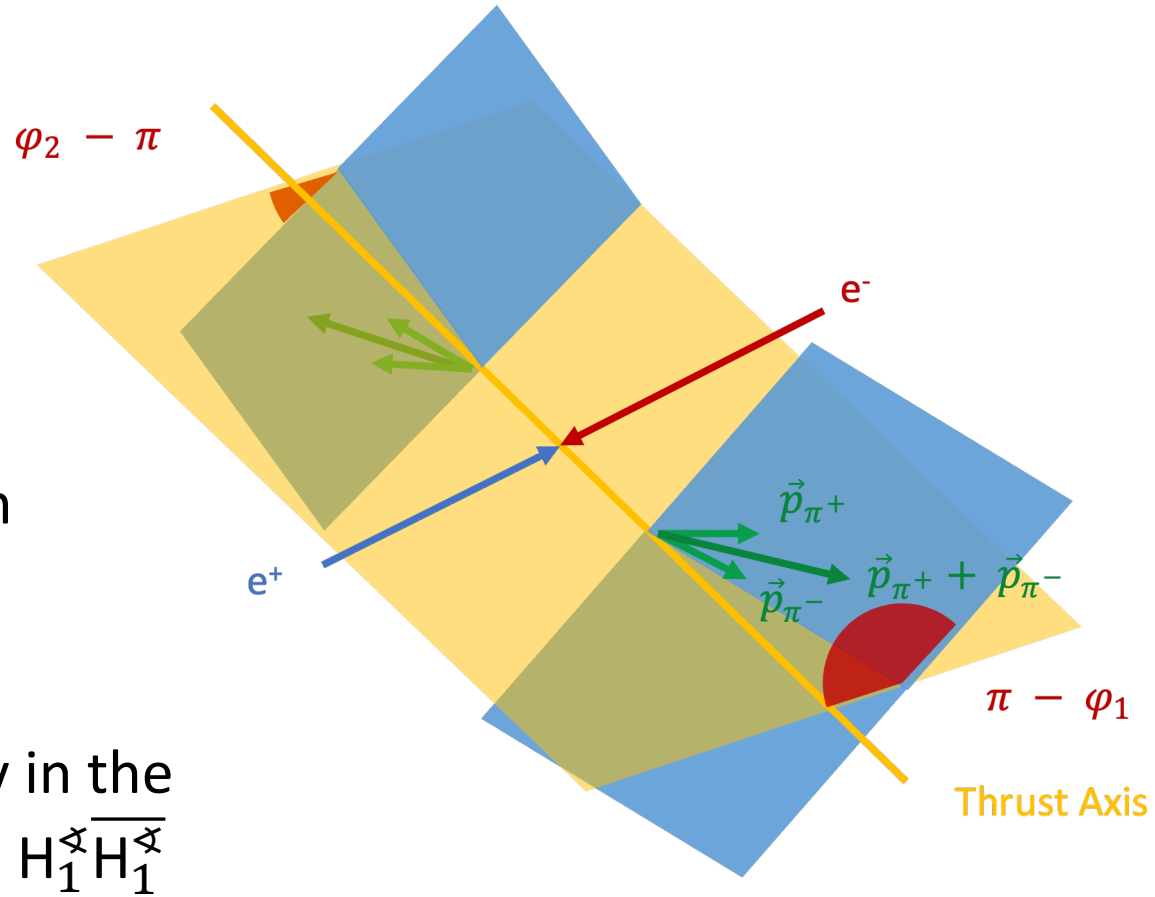

ONGOING RESEARCH

BELLE | $H_1^{\sphericalangle}$ DiFF | JET FUNCTIONS

Azimuthal Asymmetries in $e^+e^- \rightarrow (\pi^+\pi^-)(\pi^+\pi^-)$ Belle Results ($670\ fb^{-1}$):

Asymmetry by Invariant Mass Bins:

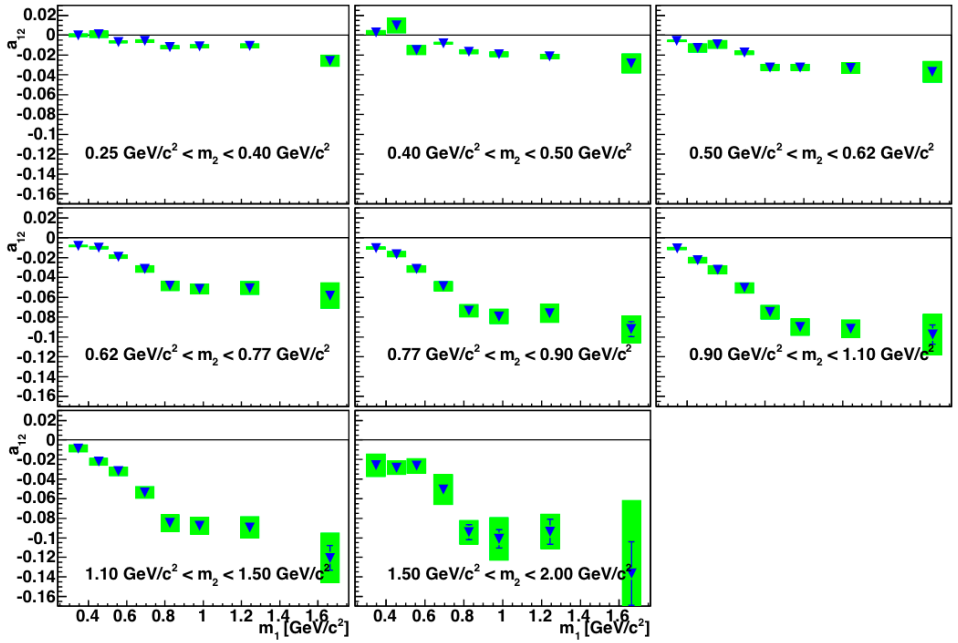

Asymmetry by Pion Fractional Energy Bins:

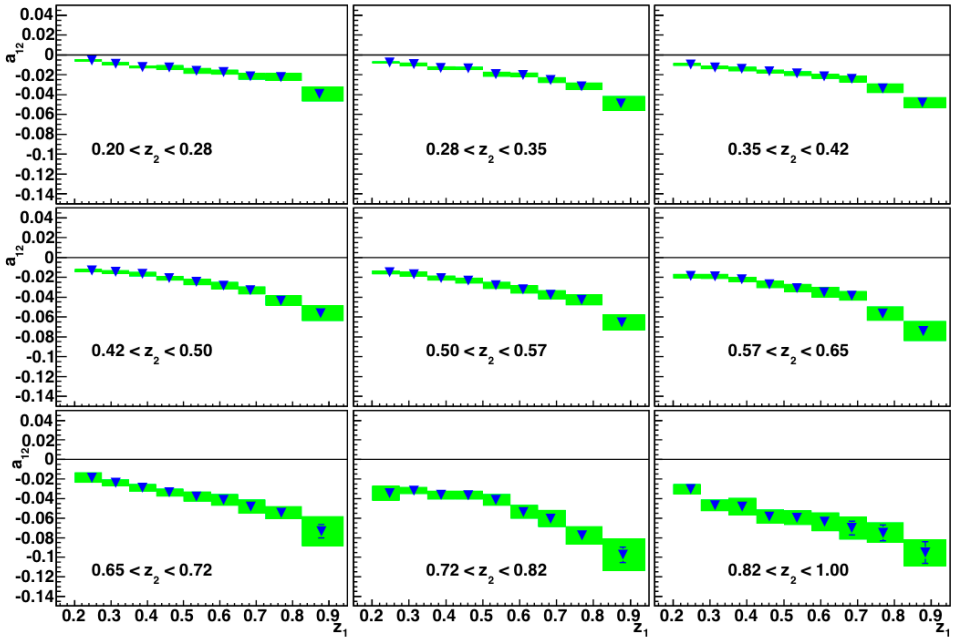

Phys. Rev. Lett. 107, 072004 (2011).

ONGOING RESEARCH

BELLE | $H_1^{\sphericalangle}$ DiFF | JET FUNCTIONS

- Kaon Inclusive
  - The same measurement of $H_1^{\sphericalangle}$ can be made with $K^+ K^-$, $K^+ \pi^-$, or $\pi^+ K^-$ pairs
  - Resulting $H_1^{\sphericalangle}$ measurements could be used to describe the distribution of strange quarks within the nucleon

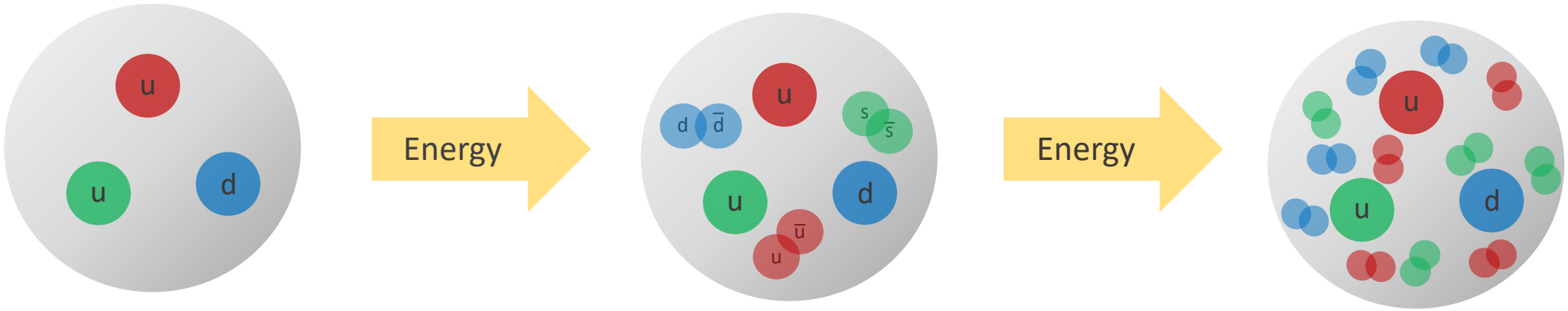

ONGOING RESEARCH

BELLE | $H_1^{\sphericalangle}$ DiFF | JET FUNCTIONS

- Kaon Inclusive
  - The same measurement of $H_1^{\sphericalangle}$ can be made with $K^+ K^-$, $K^+ \pi^-$, or $\pi^+ K^-$ pairs
  - Resulting $H_1^{\sphericalangle}$ measurements could be used to describe the distribution of strange quarks within the nucleon

- Jet Axis
  - Jets are well defined observables and produce better results than the naïve $q\bar{q}$ axis
  - Resulting FFs in e^+e^- are directly connected to FFs in SIDIS

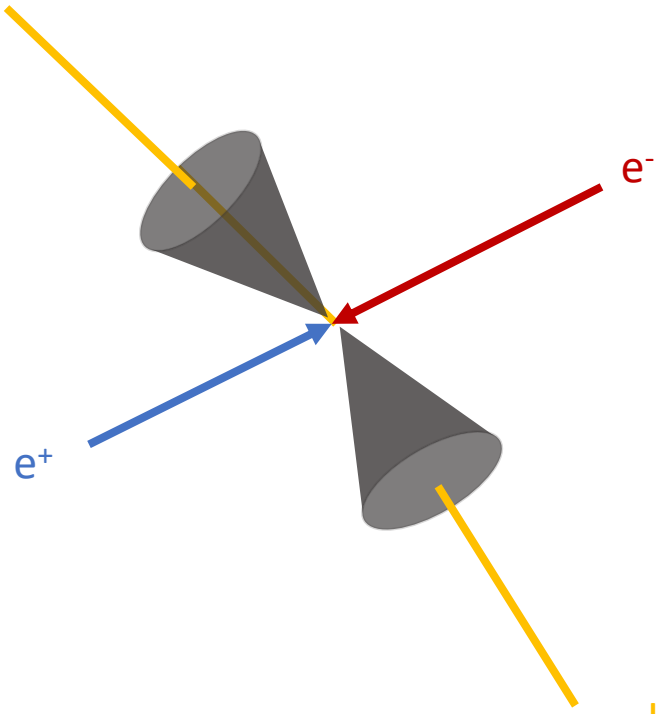

ONGOING RESEARCH

BELLE | $H_1^{\sphericalangle}$ DiFF | JET FUNCTIONS

- Kaon Inclusive
  - The same measurement of $H_1^{\sphericalangle}$ can be made with $K^+ K^-$, $K^+ \pi^-$, or $\pi^+ K^-$ pairs
  - Resulting $H_1^{\sphericalangle}$ measurements could be used to describe the distribution of strange quarks within the nucleon

- Jet Axis
  - Jets are well defined observables and produce better results than the naïve $q\bar{q}$ axis
  - Resulting FFs in e^+e^- are directly connected to FFs in SIDIS

- New measurements are critical to upcoming experiments at JLab and the EIC

ONGOING RESEARCH

BELLE | $H_1^{\sphericalangle}$ DiFF | JET FUNCTIONS

Azimuthal Asymmetries in $e^+e^- \rightarrow (\pi^+\pi^-)(\pi^+\pi^-)$ wrt the Jet Axis in Belle II Monte Carlo ($1000\ fb^{-1}$):

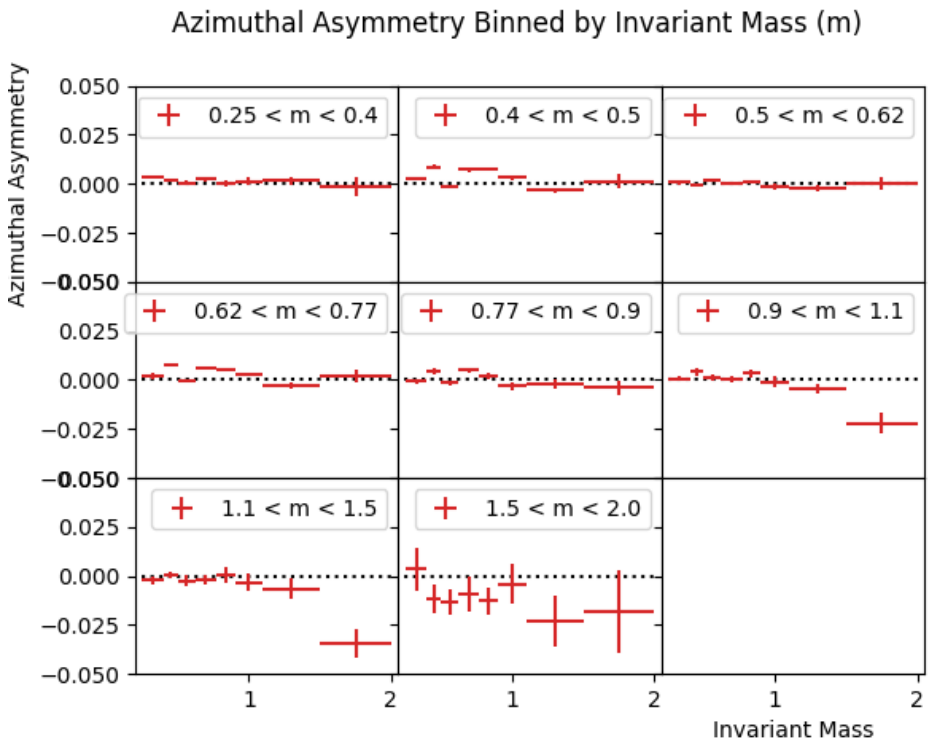

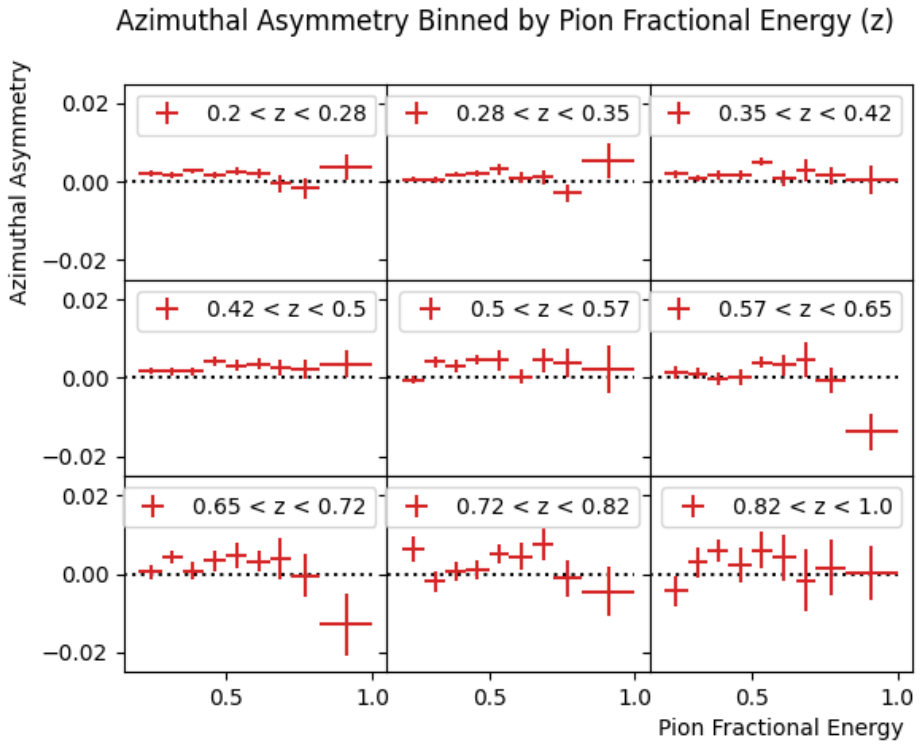

This is a consistency check; no asymmetry is expected.

ONGOING RESEARCH

- TMD FF: Transverse Momentum Dependent Fragmentation Function
- TMDs are necessary to probe the transverse momentum of quarks and gluons inside of a proton.
- Theoretically, TMD FFs can be replaced by TMD Jet Functions in factorization equations. (Gutierrez-Reyes, D., Scimemi, I., Waalewijn, W.J. *et al.)*
- TMD Jet Functions are perturbatively calculable, thus removing a source of uncertainty and allowing greater sensitivity when used to extract PDFs in SIDIS.
- At low momenta, non-perturbative corrections are larger.

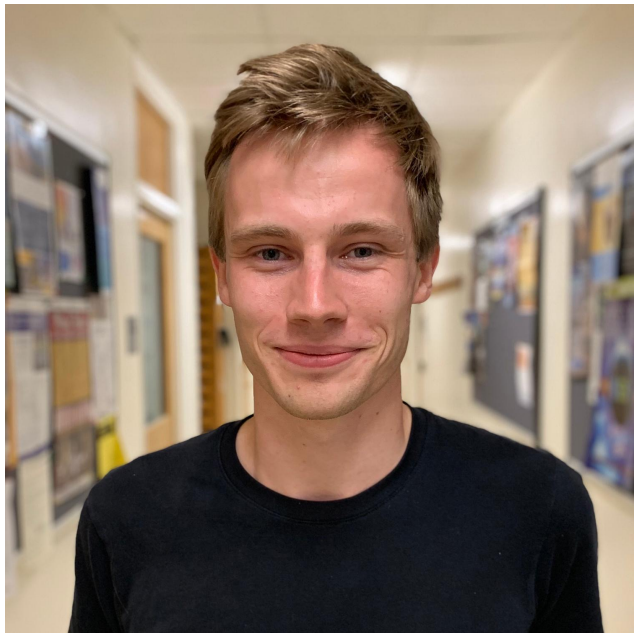

SIMON SCHNEIDER
Duke University

ONGOING RESEARCH

Measuring the jet q_T spectrum:

- Measure the transverse momentum decorrelation, $\boldsymbol{q}$, where $\boldsymbol{p}_i$ are the jet transverse momenta and z_i are their fractional energy:

$$\boldsymbol{q} = \frac{\boldsymbol{p}_1}{z_1} + \frac{\boldsymbol{p}_2}{z_2}$$

- Factorization requires the momentum decorrelation to be small:

$$q_T \equiv |\boldsymbol{q}| \ll \frac{\sqrt{s}}{2}$$

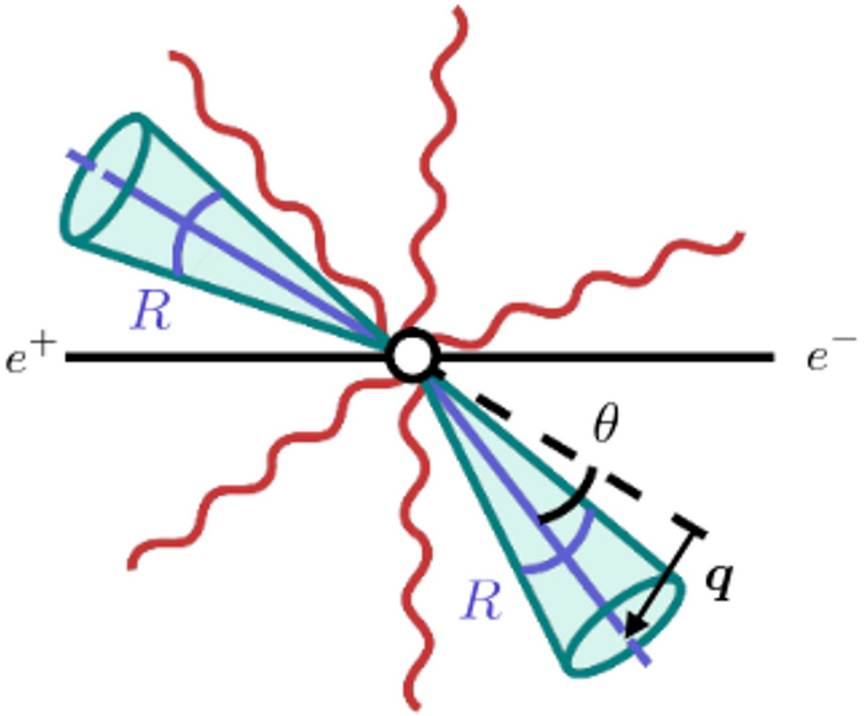

Gutierrez-Reyes, D., Scimemi, I., Waalewijn, W.J. *et al. J. High Energ. Phys.* **2019,** 31 (2019). https://doi.org/10.1007/JHEP10(2019)031

Theoretical q_T Spectrum at Belle II and LEP

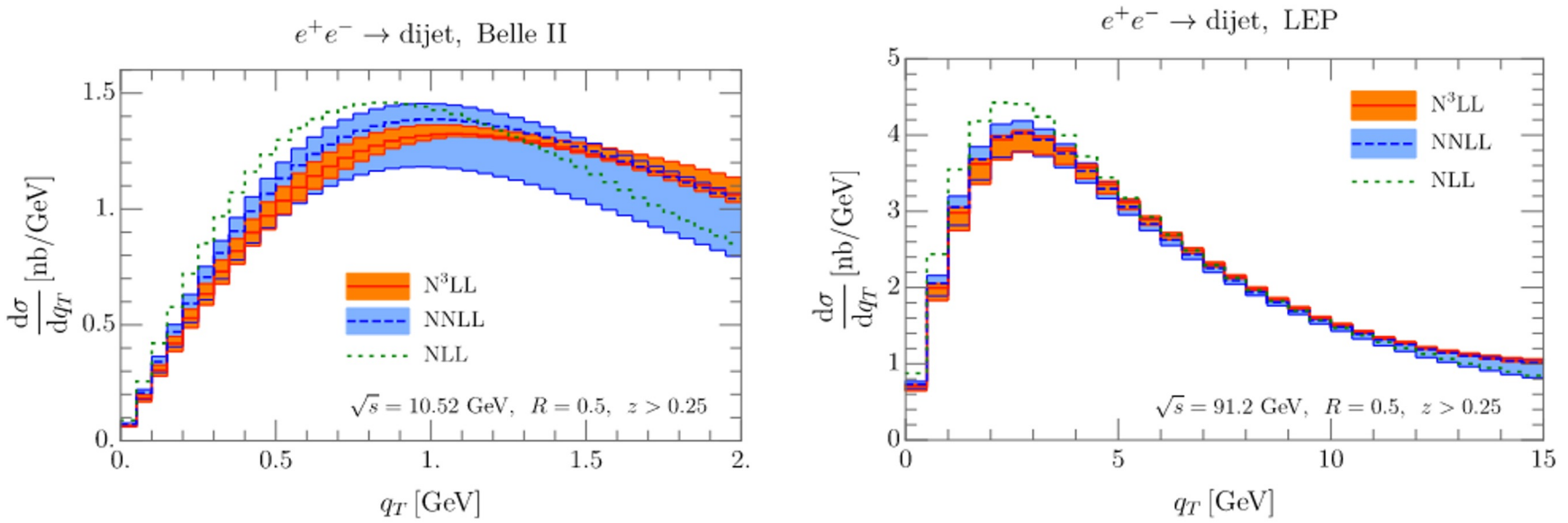

Figure 5. Perturbative convergence of the cross section differential in transverse momentum decorrelation, for Belle II (left) and LEP (right), for jet radius $R = 0.5$ and jet energy fraction $z > 0.25$. The N^{3}LL result is obtained with the prescription in eq. (6.1). The bands encode the perturbative uncertainty, as described in the text.

Gutierrez-Reyes, D., Scimemi, I., Waalewijn, W.J. *et al. J. High Energ. Phys.* **2019,** 31 (2019). https://doi.org/10.1007/JHEP10(2019)031

ONGOING RESEARCH

- The time reversal-odd (T-odd) components of a jet were thought to vanish, but were recently found to survive due to non-perturbative effects.
- T-odd jet structure plays an important role in accessing nucleon spin structures.
- In particular, the T-odd constituent can couple to the proton transversity at the EIC.

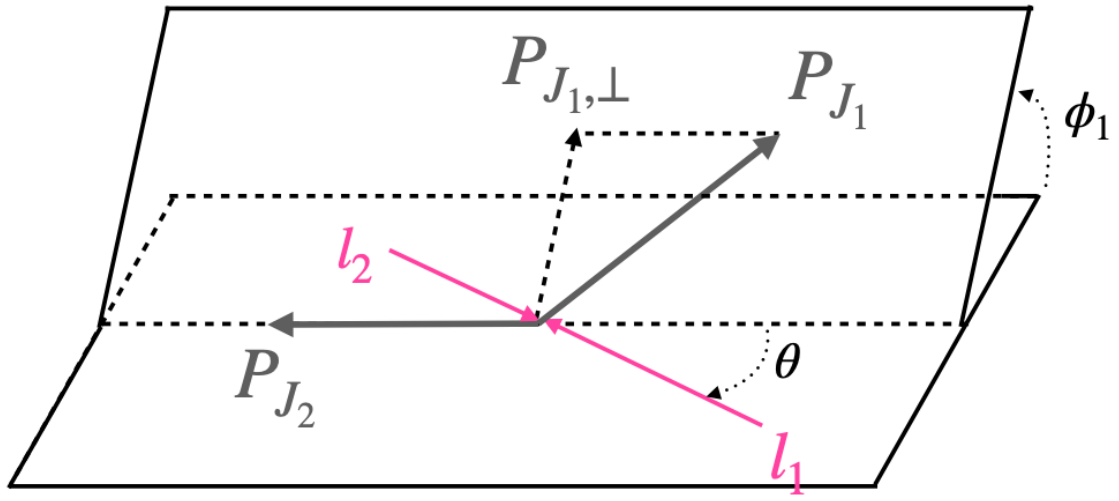

$$R^{J_1 J_2} = 1 + \cos(2\phi_1)\frac{\sin^2\theta}{1+\cos^2\theta}\frac{F_T(q_T)}{F_U(q_T)}$$

Liu, X., Xing, H. *The Time-reversal Odd Side of a Jet* arXiv:2104.03328

SUMMARY

- Fragmentation functions (FFs) are necessary to extract the nucleon structure.
- e^+e^- annihilation experiments such as Belle II provide the cleanest environment in which to measure FFs
- Ongoing FF research at Belle and Belle II
  - Vector and D meson cross section
  - Back-to-back di-hadron TMD measurements
  - A new $H_1^{\sphericalangle}$ measurement
  - Jet structure analysis

This material is based upon work supported by the National Science Foundation Graduate Research Fellowship Program under Grant No. 2139754. Any opinions, findings, and conclusions or recommendations expressed in this material are those of the author and do not necessarily reflect the views of the National Science Foundation.

BACKUP SLIDES

UPSILON RESONANCES

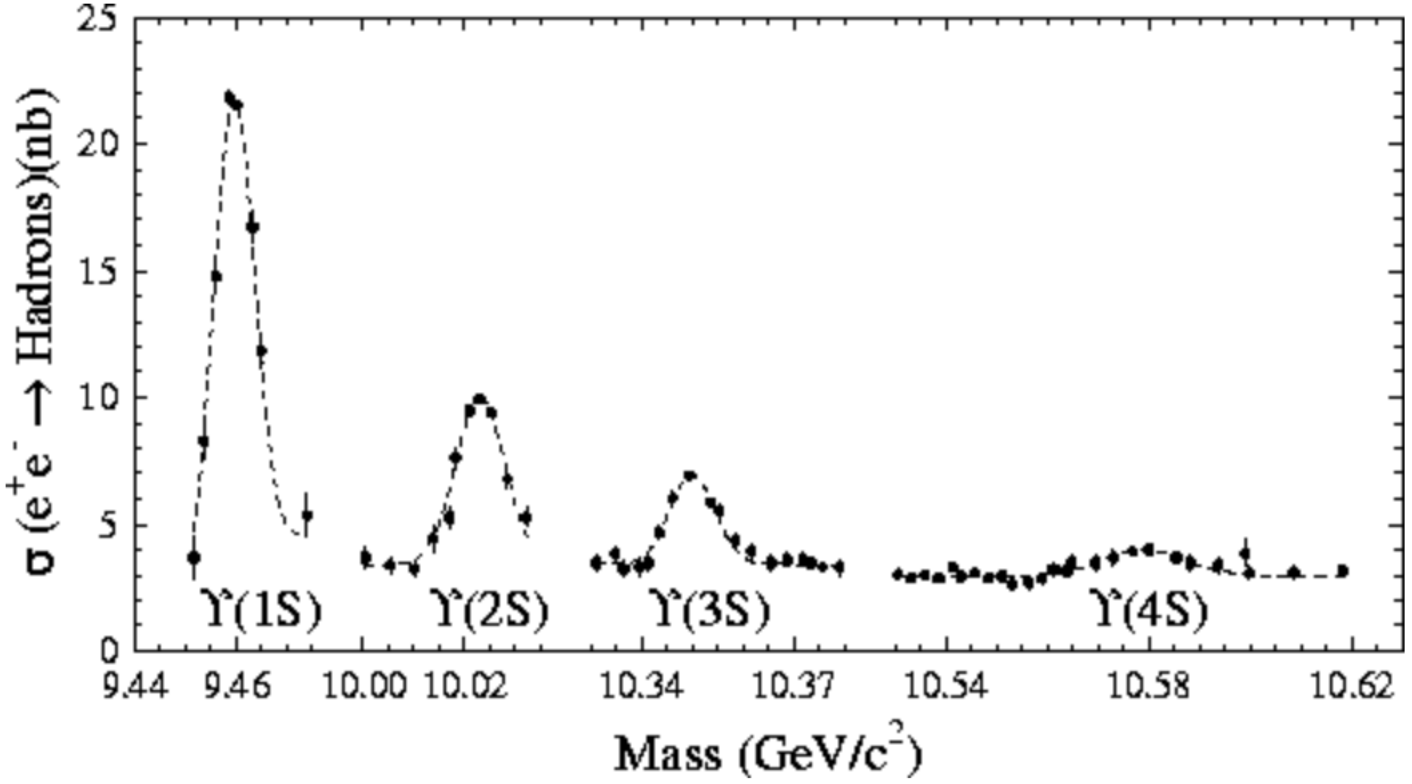

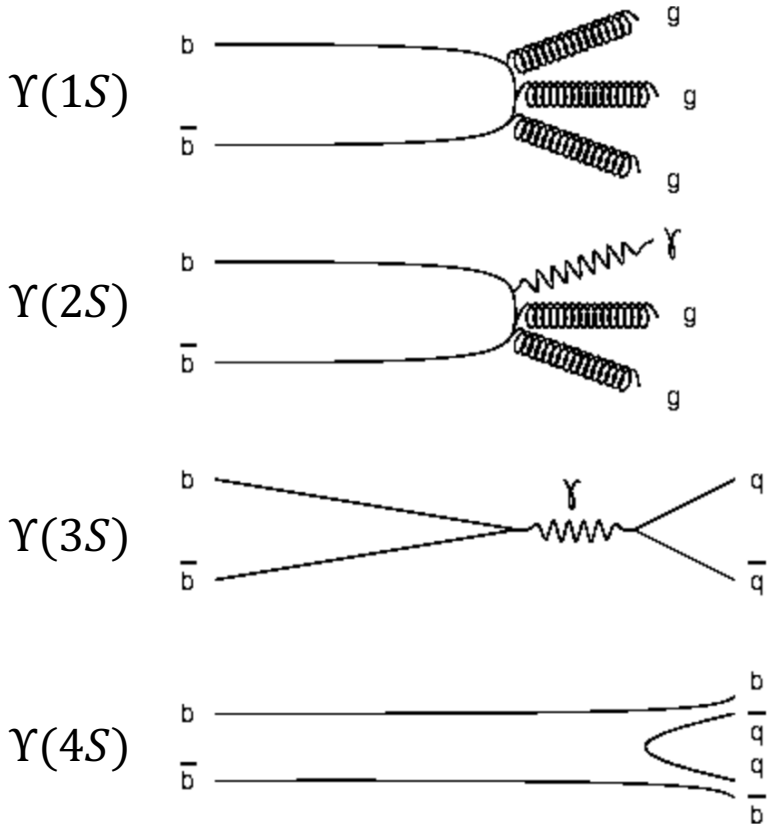

BACKUP SLIDES

FULLY DIFFERENTIAL CROSS SECTION

$$\frac{d\sigma(e^+e^-\to(h_1h_2)(\bar{h}_1\bar{h}_2)X)}{d\boldsymbol{q}_T dz d\xi dM_h^2 d\phi_R d\bar{z} d\bar{\xi} d\bar{M}_h^2 d\phi_{\bar{R}} dy d\phi^l}$$

$$= \sum_{a,\bar{a}} e_a^2 \frac{6\alpha^2}{Q^2} z^2\bar{z}^2 \Bigg\{ A(y)\mathcal{F}[D_1^a \bar{D}_1^a] + \cos(2\phi_1)B(y)\mathcal{F}\left[(2\hat{\boldsymbol{h}}\cdot\boldsymbol{k}_T\hat{\boldsymbol{h}}\cdot\bar{\boldsymbol{k}}_T - \boldsymbol{k}_T\cdot\bar{\boldsymbol{k}}_T)\frac{H_1^{\perp a}\bar{H}_1^{\perp a}}{(M_1+M_2)(\bar{M}_1+\bar{M}_2)}\right]$$

$$- \sin(2\phi_1)B(y)\mathcal{F}\left[(\hat{\boldsymbol{h}}\cdot\boldsymbol{k}_T\hat{\boldsymbol{g}}\cdot\bar{\boldsymbol{k}}_T + \hat{\boldsymbol{h}}\cdot\bar{\boldsymbol{k}}_T\hat{\boldsymbol{g}}\cdot\boldsymbol{k}_T)\frac{H_1^{\perp a}\bar{H}_1^{\perp a}}{(M_1+M_2)(\bar{M}_1+\bar{M}_2)}\right] + \cos(\phi_R+\phi_{\bar{R}}-2\phi^l)$$

$$\times B(y)|\boldsymbol{R}_T||\bar{\boldsymbol{R}}_T|\mathcal{F}\left[\frac{H_1^{\sphericalangle a}\bar{H}_1^{\sphericalangle a}}{(M_1+M_2)(\bar{M}_1+\bar{M}_2)}\right] + \cos(\phi_1+\phi_R-\phi^l)B(y)|\boldsymbol{R}_T|\mathcal{F}\left[\hat{\boldsymbol{h}}\cdot\bar{\boldsymbol{k}}_T\frac{H_1^{\sphericalangle a}\bar{H}_1^{\perp a}}{(M_1+M_2)(\bar{M}_1+\bar{M}_2)}\right]$$

$$- \sin(\phi_1+\phi_R-\phi^l)B(y)|\boldsymbol{R}_T|\mathcal{F}\left[\hat{\boldsymbol{g}}\cdot\bar{\boldsymbol{k}}_T\frac{H_1^{\sphericalangle a}\bar{H}_1^{\perp a}}{(M_1+M_2)(\bar{M}_1+\bar{M}_2)}\right] + \cos(\phi_1+\phi_{\bar{R}}-\phi^l)B(y)|\bar{\boldsymbol{R}}_T|$$

$$\times\mathcal{F}\left[\hat{\boldsymbol{h}}\cdot\boldsymbol{k}_T\frac{H_1^{\perp a}\bar{H}_1^{\sphericalangle a}}{(M_1+M_2)(\bar{M}_1+\bar{M}_2)}\right] - \sin(\phi_1+\phi_{\bar{R}}-\phi^l)B(y)|\bar{\boldsymbol{R}}_T|\mathcal{F}\left[\hat{\boldsymbol{g}}\cdot\boldsymbol{k}_T\frac{H_1^{\perp a}\bar{H}_1^{\sphericalangle a}}{(M_1+M_2)(\bar{M}_1+\bar{M}_2)}\right] + A(y)|\boldsymbol{R}_T||\bar{\boldsymbol{R}}_T|$$

$$\times\Bigg(\sin(\phi_1-\phi_R+\phi^l)\sin(\phi_1-\phi_{\bar{R}}+\phi^l)\mathcal{F}\left[\hat{\boldsymbol{h}}\cdot\boldsymbol{k}_T\hat{\boldsymbol{h}}\cdot\bar{\boldsymbol{k}}_T\frac{G_1^{\perp a}\bar{G}_1^{\perp a}}{M_1M_2\bar{M}_1\bar{M}_2}\right] + \sin(\phi_1-\phi_R+\phi^l)\cos(\phi_1-\phi_{\bar{R}}+\phi^l)$$

$$\times\mathcal{F}\left[\hat{\boldsymbol{h}}\cdot\boldsymbol{k}_T\hat{\boldsymbol{g}}\cdot\bar{\boldsymbol{k}}_T\frac{G_1^{\perp a}\bar{G}_1^{\perp a}}{M_1M_2\bar{M}_1\bar{M}_2}\right] + \cos(\phi_1-\phi_R+\phi^l)\sin(\phi_1-\phi_{\bar{R}}+\phi^l)\mathcal{F}\left[\hat{\boldsymbol{g}}\cdot\boldsymbol{k}_T\hat{\boldsymbol{h}}\cdot\bar{\boldsymbol{k}}_T\frac{G_1^{\perp a}\bar{G}_1^{\perp a}}{M_1M_2\bar{M}_1\bar{M}_2}\right] + \cos(\phi_1-\phi_R+\phi^l)$$

$$\times\cos(\phi_1-\phi_{\bar{R}}+\phi^l)\mathcal{F}\left[\hat{\boldsymbol{g}}\cdot\boldsymbol{k}_T\hat{\boldsymbol{g}}\cdot\bar{\boldsymbol{k}}_T\frac{G_1^{\perp a}\bar{G}_1^{\perp a}}{M_1M_2\bar{M}_1\bar{M}_2}\right]\Bigg)\Bigg\},$$

$\boldsymbol{R}_T$: The transverse part of the relative momentum between the hadrons

$M_{1,2}$: Mass of hadron 1,2

$\phi_R - \phi^l$: The azimuthal angle with respect to the lepton frame

A kinematic factor dependent only on θ in the center of mass frame:

$$B(y) = \frac{sin^2\theta}{4}$$

$\mathcal{F}$: The convolution

D. Boer, R. Jakob, and M. Radici, Phys. Rev. D 67, 094003 (2003).

BACKUP SLIDES

SUPERKEKB NANOBEAM SCHEME

- Luminosity (L):

$$L \propto \frac{I_{\pm}\xi_{y\pm}}{\beta^*_{y\pm}}$$

- Vertical beta function at the interaction point ($\beta^*_{y\pm}$) decreased by a factor ~20
- Hourglass condition where d is the overlap region between bunches:

$$\beta^*_{y\pm} > d$$

	KEKB Achieved	SuperKEKB
Energy (GeV) (LER/HER)	3.5/8.0	4.0/7.0
ξ_y	0.129/0.090	0.090/0.088
β^*_y (mm)	5.9/5.9	0.27/0.41
I (A)	1.64/1.19	3.60/2.62
Luminosity ($10^{34}\mathrm{cm}^{-2}\mathrm{s}^{-1}$)	2.11	80

BACKUP SLIDES
VERTEX DETECTOR

- Main purpose is to measure decay vertices for B-mesons, D-mesons, and τ-leptons
- Innermost subdetector at Belle II
- The Pixel Detector (PXD):
  - 2 layers of silicon pixels
  - Developed to handle the high backgrounds at Belle II
- The Silicon Vertex Detector (SVD):
  - 4 layers of double sided silicon strips

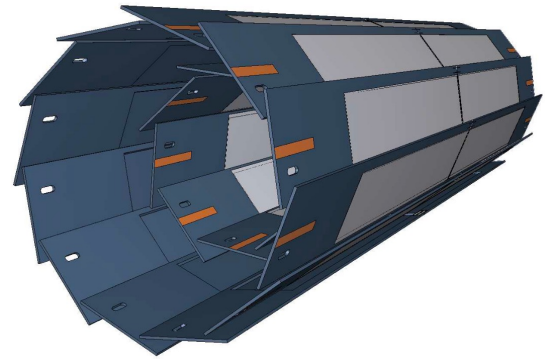

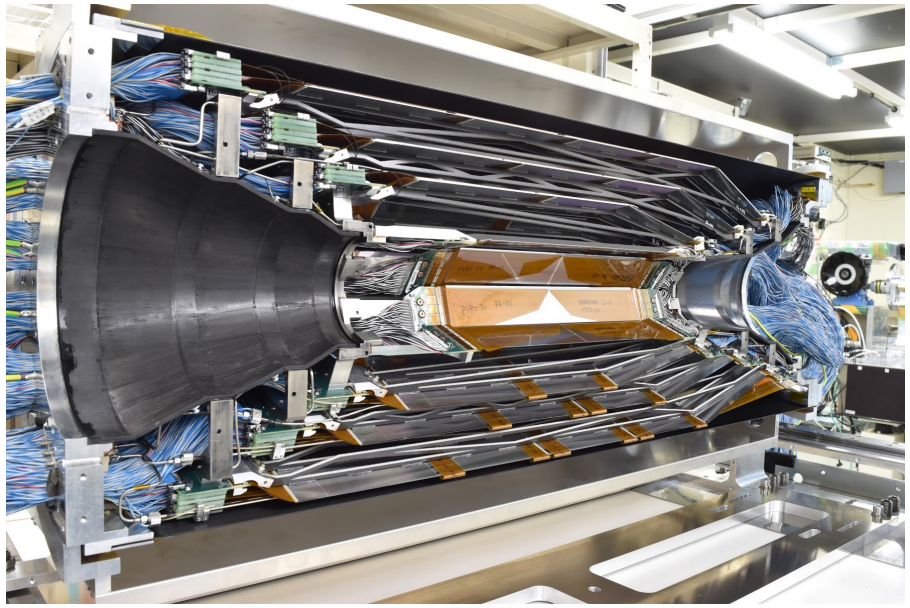

BACKUP SLIDES

CENTRAL DRIFT CHAMBER

- Reconstructs charged tracks and measures their momenta
- Provides energy loss measurements used for particle identification
  - Particularly important for low momentum tracks that do not reach the PID
- Provides trigger signals for charged particles
- Contains 14,336 wires in axial or stereo orientation
  - axial: aligned with the solenoidal magnetic field
  - stereo: skewed with respect to the axial wires

BACKUP SLIDES

TIME OF PROPAGATION CHAMBER

- Identifies charged particles in the barrel region by imaging the Cherenkov rings produced by those particles.
- Photons reach PMTs after total internal reflection down the quartz radiator bar
- Positions and arrival times of photons in the TOP detector are used to calculate a likelihood for a given particle mass hypothesis.
- It is the only existing and operational time-of-propagation counter and the first to be used in a collider experiment.

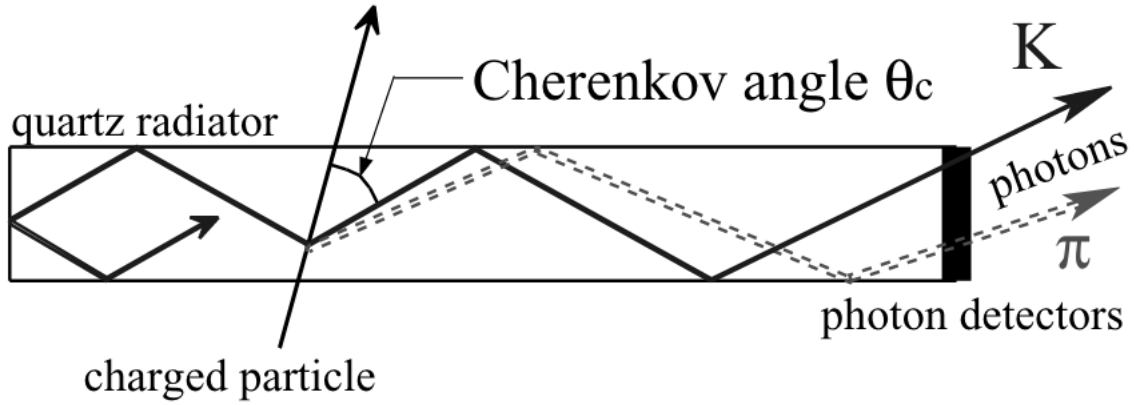

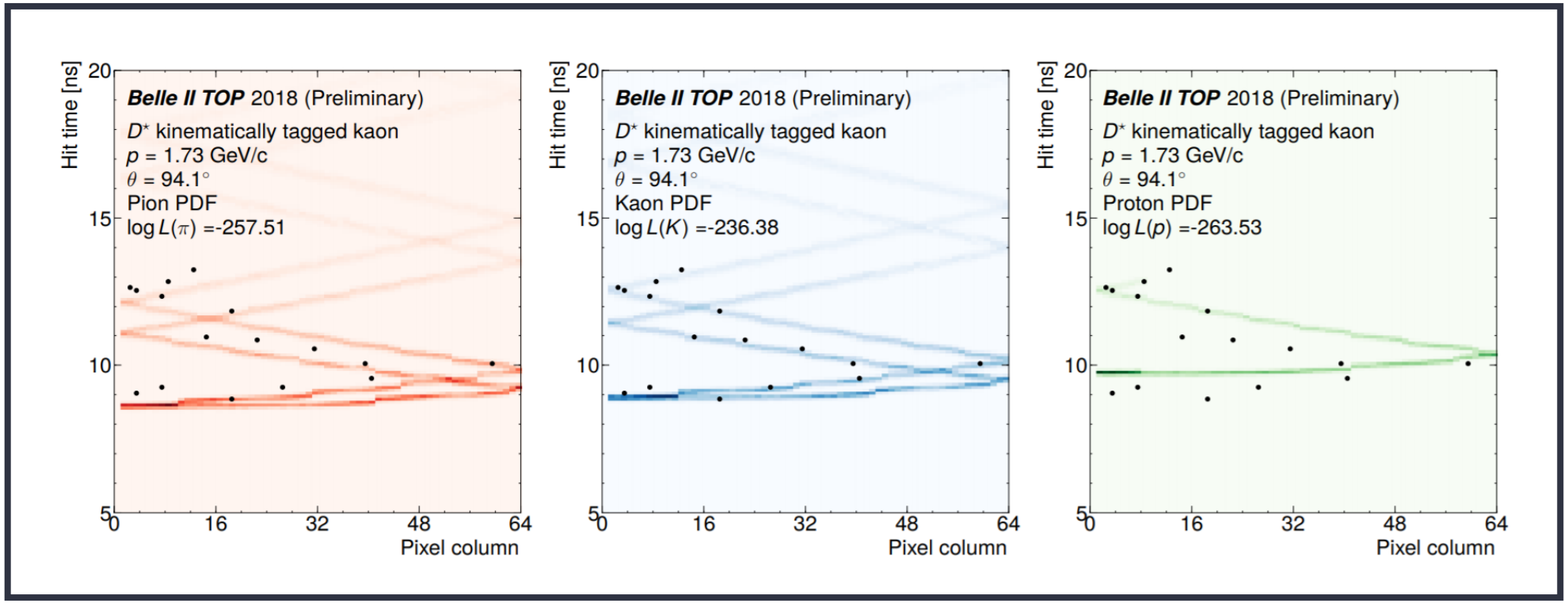

KAON DATA IN TOP

BACKUP SLIDES

AEROGEL RING IMAGING CHERENKOV DETECTOR

- Identifies charged particles in the endcap region by imaging the Cherenkov rings produced by those particles.
- Contains 124 pairs of aerogel tiles used as radiators
  - Two layers of aerogel with different refractive indices are used to increase the yield without degrading the Cherenkov angle resolution.
- The Cherenkov angle can be calculated from the radius of the Cherenkov ring and is used to calculate the mass of the charged particle by the following formula:

$$m = \frac{p}{c}\sqrt{n^2 cos^2\theta_C - 1}$$

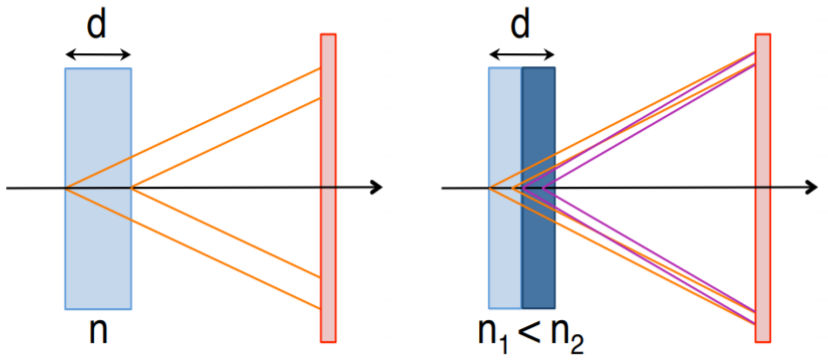

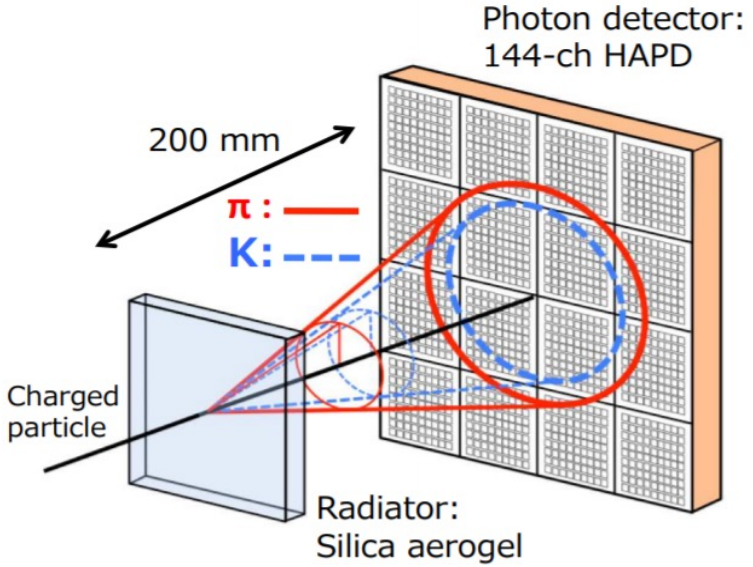

BACKUP SLIDES

ELECTROMAGNETIC CALORIMETER

- Measures the energy of electromagnetically interacting particles
- Used to identify electrons and photons
- Helps identify K_L mesons
- An array of 8,736 CsI(Tl) crystal that covers the barrel region as well as both endcap regions

BACKUP SLIDES

K_L MUON DETECTOR

- The KLM is used primarily to identify K_L mesons and muons.
- Iron plates provide 3.9 hadronic interaction lengths of material.
  - Muons and other non-showering charged hadrons move through the KLM in straight lines.
  - K_L mesons interact in the ECL or with the iron plates of the KLM creating showers.
- Increased backgrounds and resistive plate chamber (RPC) deadtimes could drastically decrease efficiency
- Endcap and interior barrel RPCs were replaced with plastic scintillator
  - Shorter deadtimes
  - Provides neutron shielding

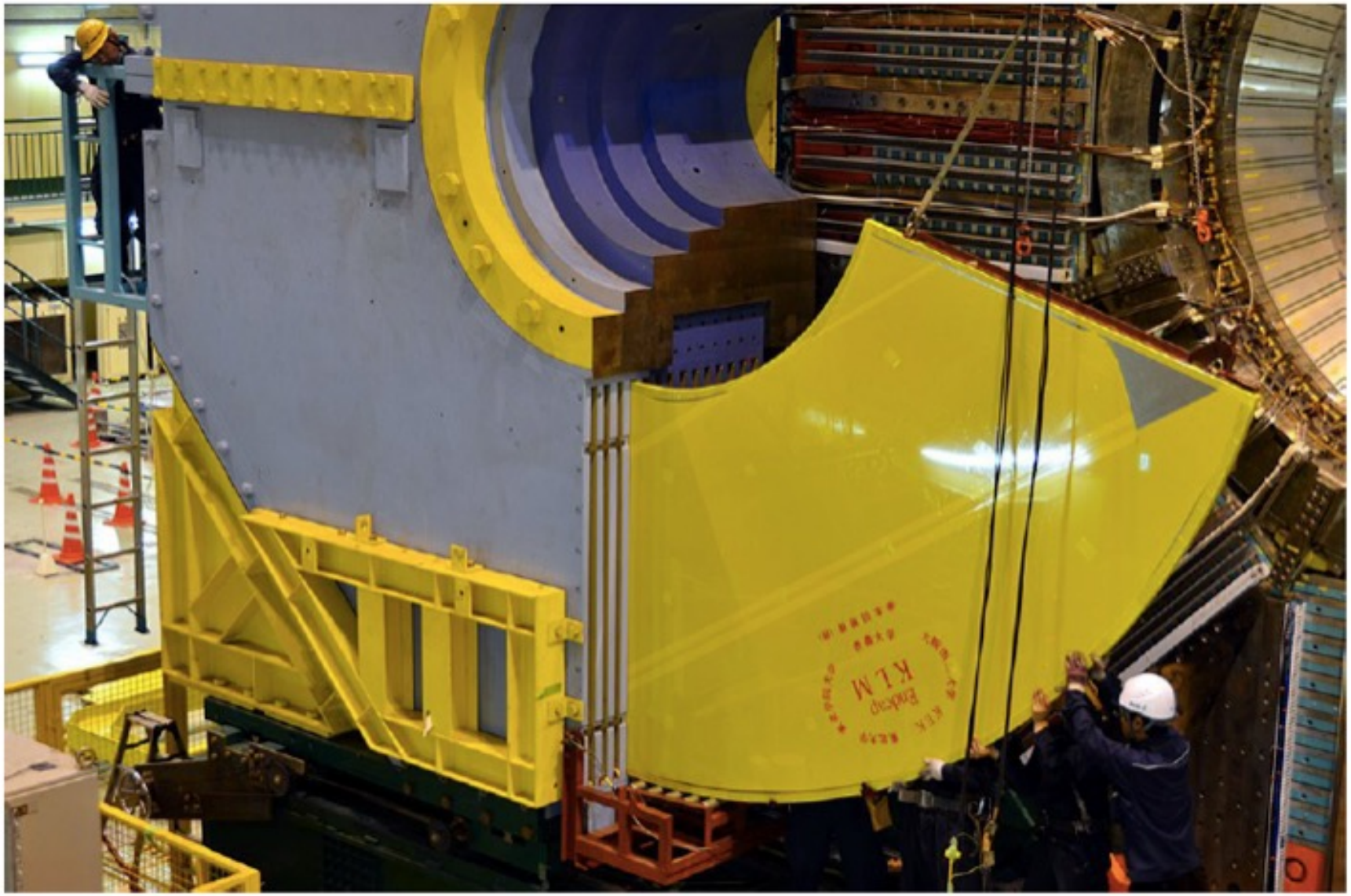

KLM ENDCAP

BACKUP SLIDES

K_L MUON DETECTOR

- The KLM barrel has 15 layers:
  - 13 Resistive Plate Chamber (RPC) layers
  - 2 scintillators layers
- Inner layers of the KLM were replaced with scintillator to reduce deadtime.

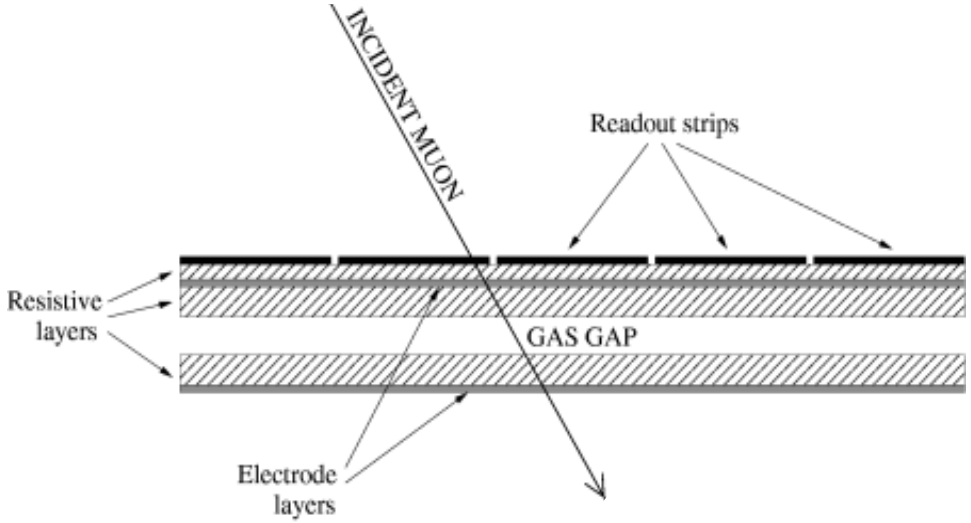

RPC

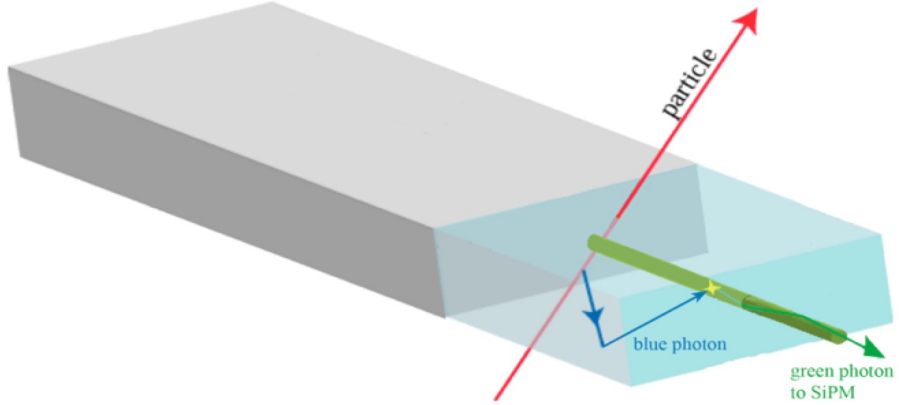

SCINTILLATOR

Anti-k_t algorithm for e^+ e^- :

1. For each pair of "particles" i and j, find the k_t distance between them:

$$d_{ij} = \min\left(E_i^{-2}, E_j^{-2}\right)\frac{\left(1-\cos\theta_{ij}\right)}{(1-\cos R)}$$

2. For each "particle" i, find the beam distance:

$$d_{iB} = E_i^{-2}$$

3. Find the minimum of all d_{ij} and d_{iB} values that were calculated.
   If it is a d_{ij} value → merge "particles" i and j
   If it is a d_{iB} value → complete the jet and remove it from the list

4. Repeat until no "particles" are left in the list

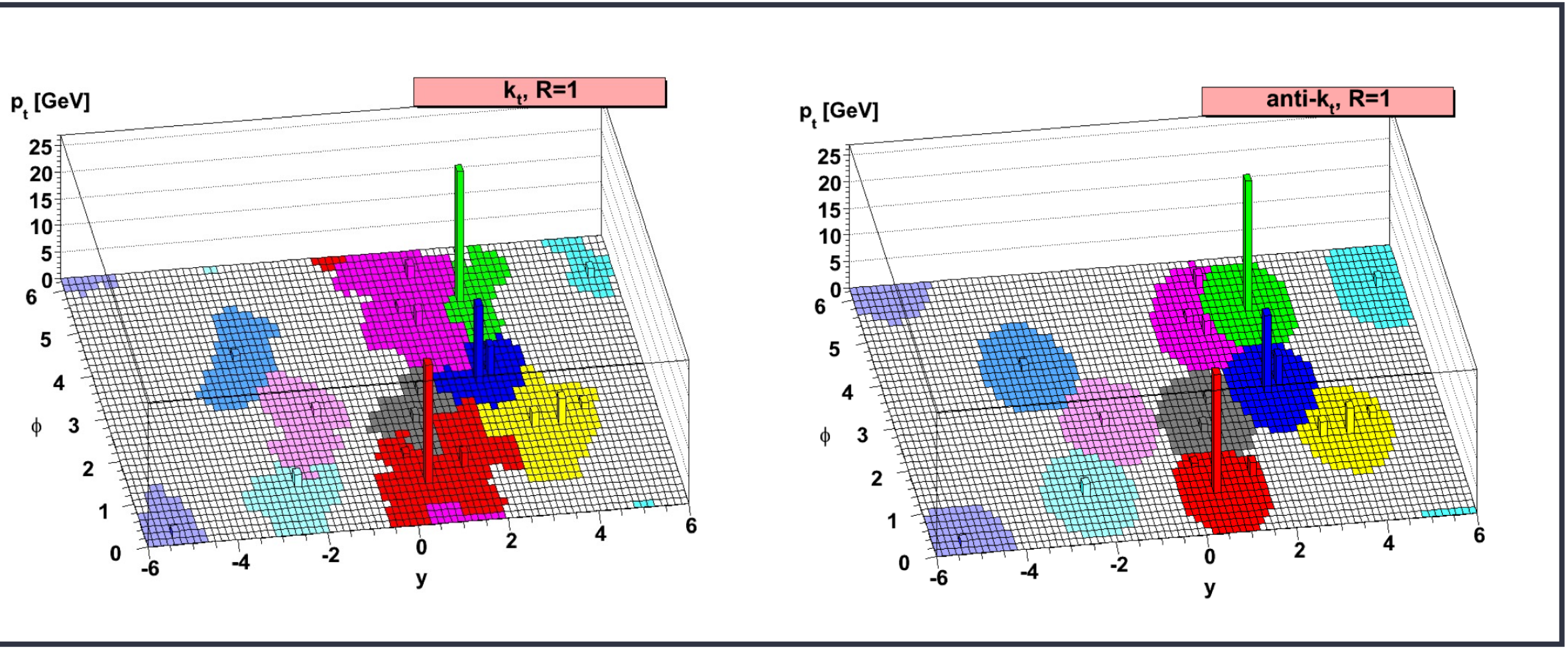

JET ALGORITHM COMPARISON [3]

Standard jet axis (SJA) recombination:

When particles are merged, their 4-vectors are simply added:

$$\vec{p}_{12} = \vec{p}_1 + \vec{p}_2$$

Winner-takes-all (WTA) recombination:

The resulting combined particle is massless and its direction is defined to be the same as the highest momentum constituent particle:

$$\vec{p}_{12} = E_{12}\left[\frac{\vec{p}_1}{|\vec{p}_1|}\theta(E_1 - E_2) + \frac{\vec{p}_2}{|\vec{p}_2|}\theta(E_2 - E_1)\right]$$

BACKUP SLIDES

WTA UUBAR MC BINNING

z

m

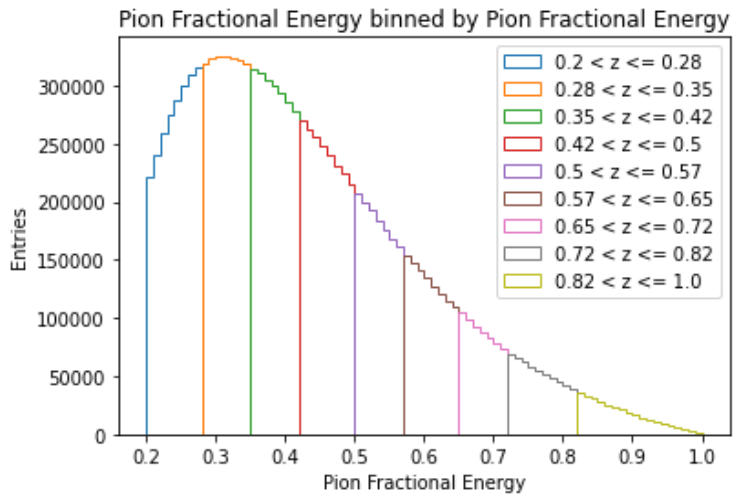

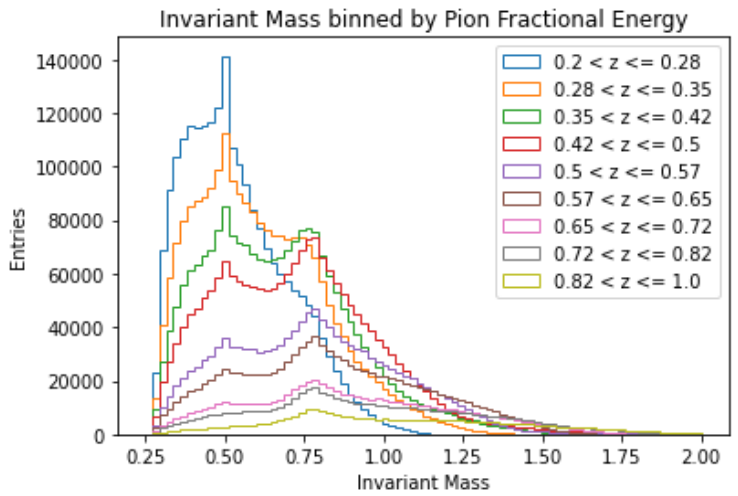

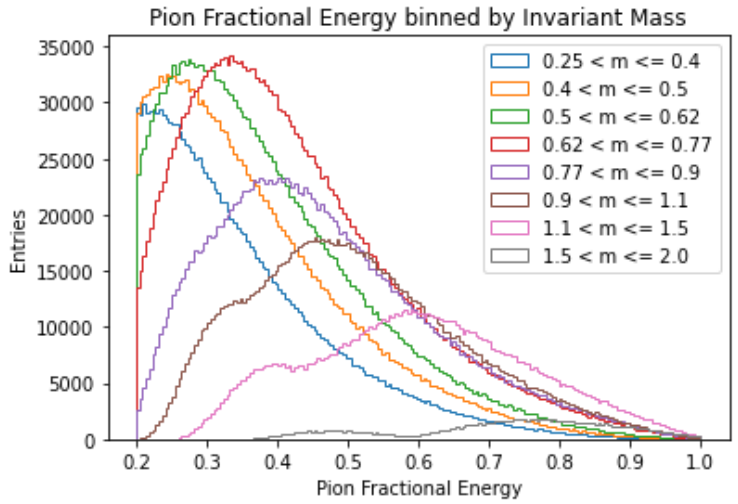

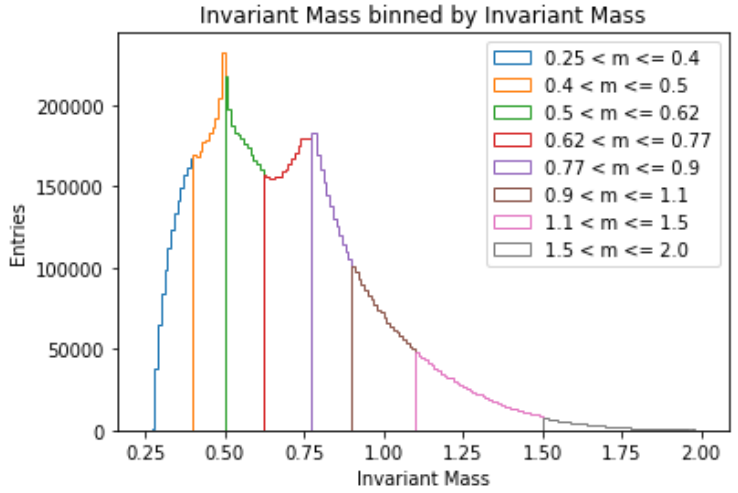

BACKUP SLIDES

JET HANDEDNESS

- Longitudinal jet handedness:

$$H_{\parallel} = \frac{N_L(n_{\parallel} > 0) - N_R(n_{\parallel} < 0)}{N}$$

- Transverse jet handedness:

$$H_{\perp} = \frac{N_L(n_{\perp}^{\sigma} > 0) - N_R(n_{\perp}^{\sigma} < 0)}{N}$$

- Total number of events is the sum of left-handed and right-handed events: $N = N_L + N_R$
- $n_{\parallel} \propto \epsilon_{ijk} k^i k_1^j k_2^k$
- $n_{\perp}^{\sigma} \propto \epsilon_{ijk} e_{\perp}^{\sigma,i} k_1^j k_2^k$ where $\sigma = 1,2$
- The momenta of the hadrons is $k_{1,2}$, the longitudinal momentum of the jet is k, and the transverse momentum of the jet is $e_{\perp}^{\sigma}$
- The two leading hadrons have to be ordered the same way in all events, either by their charges or by the magnitude of their momenta

ONGOING RESEARCH

Azimuthal Asymmetry from $q\bar{q}$ in Belle II Monte Carlo (200 fb^{-1})

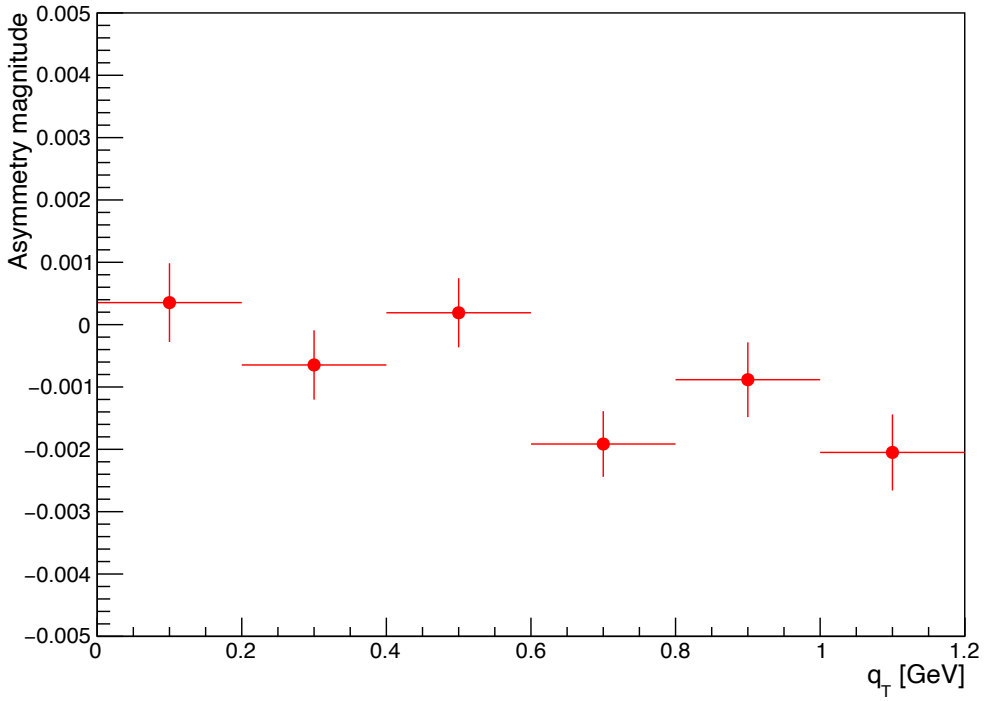

This is a consistency check; no asymmetry is expected.

FRAGMENTATION FUNCTIONS

INTRODUCTION

OUR GOAL

We want to know how quark properties lead to larger scale effects like hadron distribution and polarization.

Jet: a collimated bunch of colorless, bound hadronic states